THE MECHANICAL UNFOLDING OF FIBRONECTIN USING ATOMIC FORCE MICROSCOPY AND ITS RELEVANCE TO BIOCOMPATIBILITY STUDIES

by

Pamela Yvonne Meadows

BS, Concord College, 2000

MS, University of Pittsburgh, 2003

Submitted to the Graduate Faculty of

University of Pittsburgh in partial fulfillment

of the requirements for the degree of

Doctor of Philosophy

University of Pittsburgh

2005

UNIVERSITY OF PITTSBURGH

FACULTY OF ARTS AND SCIENCES

This dissertation was presented

by

Pamela Yvonne Meadows

It was defended on

May 25, 2005

and approved by

Professor Toby Chapman

Professor Sunil Saxena

Professor William Wagner

Professor Gilbert Walker
Dissertation Director

ACKNOWLEDGEMENTS

THE MECHANICAL UNFOLDING OF FIBRONECTIN USING ATOMIC FORCE MICROSCOPY AND ITS RELEVANCE TO BIOCOMPATIBILITY STUDIES

Pamela Yvonne Meadows, PhD

University of Pittsburgh, 2005

ABSTRACT

Protein adsorption to surfaces has hindered advancements made in biocompatible implants and drug delivery. Once a protein adsorbs, it can undergo conformational changes and unfold to expose buried cryptic sites of the protein. These sites are often critical for signaling additional proteins and cells to adsorb to the surface which can eventually lead to an implant's failure or the destruction of drug delivering devices. To improve the biocompatibility of these implants, an understanding of how a surface affects a protein's conformation and stability is required. In this work, an atomic force microscope (AFM) is used to quantify the stability of fibronectin (FN), an adhesion promoting protein, on mica, gold, poly(ethylene glycol), and $-CH_3$, $-OH$, and $-COOH$ terminated alkanethiol self-assembled monolayers. The thermodynamic parameters associated with this mechanically induced denaturation are presented as a function of surface type and amount of adsorbed protein using two different models. Results indicate greater stabilization of FN in densely deposited films while greater surface denaturation occurs as the proteins become more isolated on the substrate. Additional information about the protein's binding state was also obtained. Proteins aggregated on a hydrophobic surface adopted more rigid conformations apparently as a result of increased surface denaturation and tighter binding while looser conformations were observed on more hydrophilic surfaces. Finally, the force spectroscopy experiments were examined for any biocompatibility correlation by seeding substrates with

human umbilical vascular endothelial cells (HUVEC). As predicted from the models used in this work, surfaces with aggregated FN promoted cellular deposition while surfaces with proteins sparsely populated hindered cellular deposition and growth. The AFM's use as a means for projecting cell deposition and perhaps biocompatibility does look promising.

TABLE OF CONTENTS

LIST OF TABLES

LIST OF FIGURES

1.   INTRODUCTION

1.1.   ATOMIC FORCE MICROSCOPY

Since its invention in the 1980s, the atomic force microscope (AFM) has become a widely used tool for measuring both intra- and intermolecular interactions. A few of the more common areas explored with an AFM include ligand-receptor adhesion forces,[1] polymer elasticity[2-6] and conductivity,[7] DNA[8] and RNA[9] folding kinetics, and the elastic properties of proteins in the extracellular matrix.[10-14] In this work, we use AFM as a single-molecule probe to study the mechanical properties of fibronectin (FN). Information about the protein's conformational state can also be obtained from images collected in an intermittent contact mode. Details about this procedure and the basic instrumental setup can be found below. It is important to note that in order to visualize a protein's conformational state, ultra-flat surfaces must be prepared since a protein's height may only be a couple of nanometers (nm). A technique to prepare gold surfaces with a root-mean-square roughness (RMS) of less than 0.3 nm is also described.

1.1.1.   Surface Imaging

A schematic of the major components in an AFM can be found in Figure 1. During imaging, a cantilever with a small tip scans across the surface while the detector collects the changes in the

laser position due to bending of the cantilever. The imaging can be done in one of two modes: contact mode where the feedback loop attempts to maintain a constant deflection or intermittent contact where the tip is driven at its resonant frequency and the feedback loop attempts to maintain a constant amplitude set by the user. Intermittent contact, as used in this work, allows biological samples to be studied without damaging the specimen making it the mode of choice. This is possible since the tip spends less time in contact with the sample.
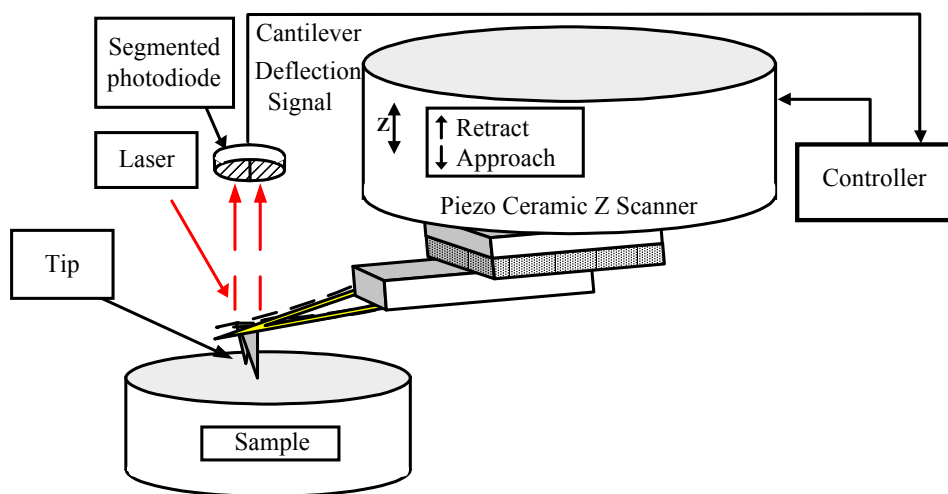
Figure 1 A schematic of an atomic force microscope. Deflections of the laser beam, due to cantilever bending, are collected by a segmented photodiode detector. The signals are then sent to a controller which directs the movement of the piezo. For imaging purposes, two other piezo's are installed allowing 3-dimensional scanning of the surface.

1.1.2. Protein Unfolding

To study the mechanical properties of adsorbed FN, the AFM was operated primarily in force mode, a 1-dimensional mode of imaging allowing the force as a function of tip-sample

separation to be determined. Figure 2 shows a schematic of a typical force plot obtained on a bare surface using this mode of imaging. Here, the piezo extends toward the surface (noted by the red line) until it comes into contact with the substrate (B). The tip continues to press into the surface resulting in an increase in deflection until the piezo has extended to a predetermined value set by the user. The piezo then begins to retract and when the adhesive forces are exceeded by the pulling force (as seen by point D), the tip breaks free from the surface and the deflection returns to zero.
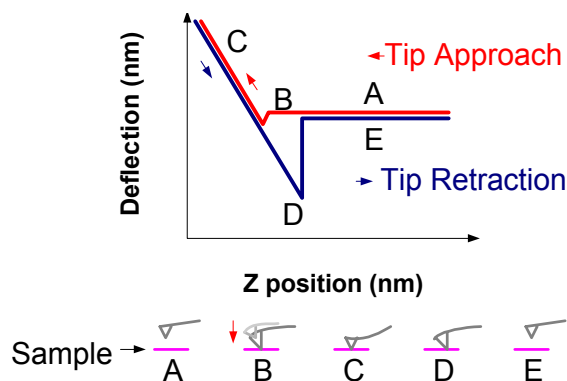
Figure 2 A schematic showing a tip's response at different regions of a force plot on a bare substrate.

When a protein such as FN absorbs onto the AFM tip, the protein can be elongated as the piezo retracts. An illustration of this mechanical unfolding can be seen in Figure 3 while Figure 4 displays the corresponding force plot obtained for the extension of a two domain protein. During the extension of the protein, a point is reached when the pulling force exceeds the force needed to rupture the least stable domain, and the unfolding of that domain occurs as seen by number 3 in Figures 3 and 4. Rupturing of the domain adds significant length to the extended protein and

this added length is stretched out as the piezo continues to retract. This process of domain denaturation is repeated until the domains between the tip and surface are all denatured, provided the adhesion force between the tip and protein exceeds the rupture forces of these domains. As can be seen in Figure 3, once the protein detaches from the tip, the domains can refold. It is also necessary to point out that force plots can give an indication of the length of the domain that was ruptured. The difference in length between successive pulling events is an approximation of the length of the domain; the actual length of the domain cannot be determined since the protein is not completely extended due to entropic factors.
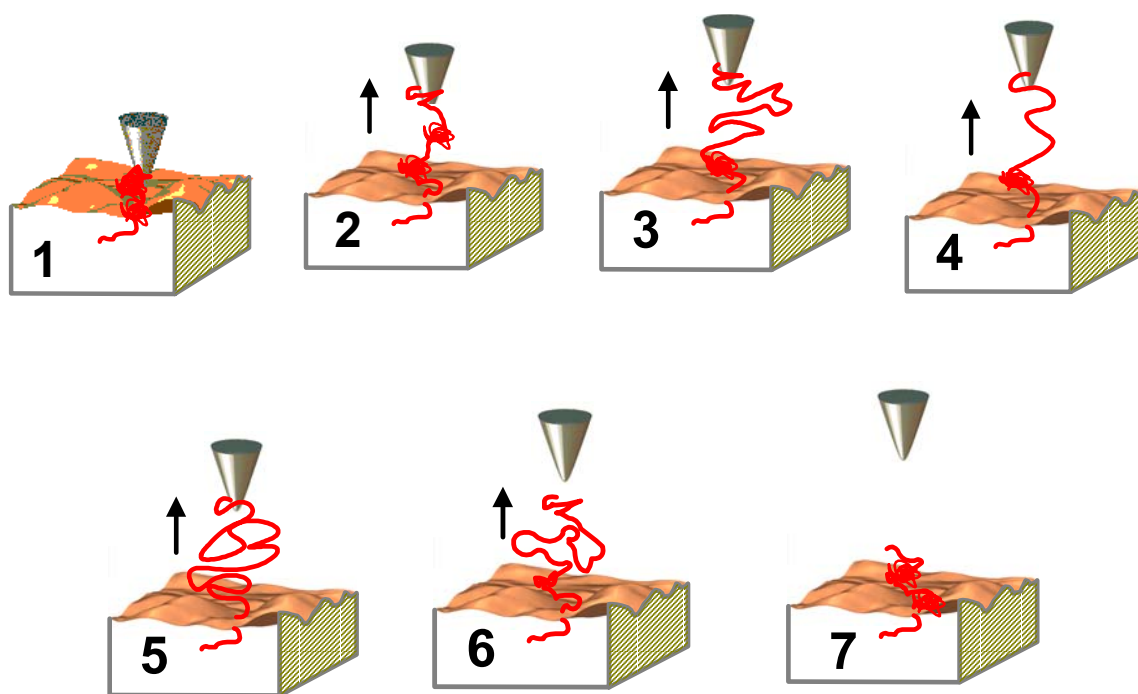
Figure 3 A schematic of protein unfolding. As the tip approaches in step 1, the protein can physisorb to the tip and then become elongated. As long as the adhesion between the tip and protein is strong enough, domain denaturation events can then be observed as seen in steps 3 and 5. After elongation of the unfolded domains, the protein will break away from the tip and eventually refold.
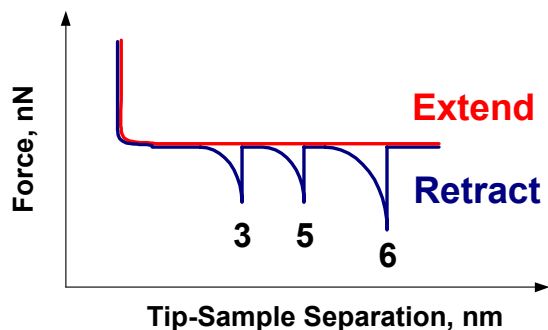
Figure 4 The first two ruptures represent domain unfolding while the last rupture represents a protein-tip rupture. The numbers correspond to the schematics drawn in Figure 3.

1.2. FIBRONECTIN

Fibronectin is a large adhesion promoting protein composed of 2,446 amino acids with a molecular weight of 450 kDa. It has two similar polypeptide chains that are linked near their carboxy termini via disulfide bonds. In its partially denatured form, the protein is approximately 140 nm in length with a width of 2 nm. A schematic of this more extended conformation can be seen in Figure 5. Each monomer of this protein is composed of 12 Type I, 2 Type II, and 17 Type III domains. Both the Type I and Type II domains possess disulfide bonds whose strength precludes their mechanical denaturation in the force-extension experiments reported here; however, the Type III domains, which lack disulfide bonds, can be mechanically denatured, and it is also these domains that are responsible for cellular binding. Because FN is a major adhesion promoting protein, it is imperative that we understand the adsorption of this protein on surfaces designed for biomedical applications.
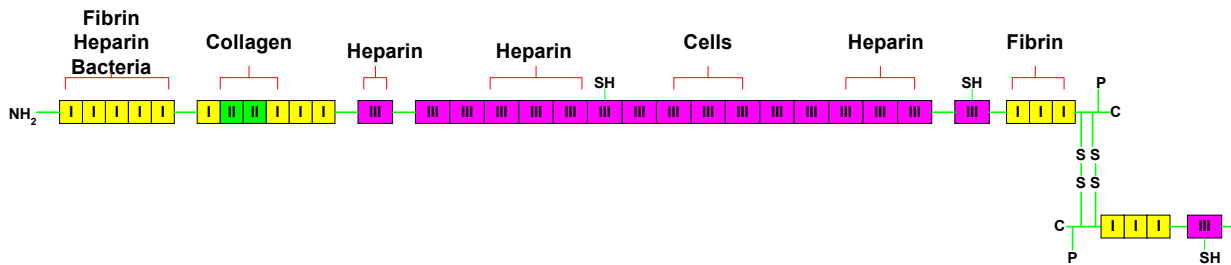
Figure 5 A schematic of a FN monomer displaying the binding sites of several molecules.

1.3. PREPARATION OF ULTRA-FLAT GOLD SURFACES

As mentioned previously, proteins can adopt surface conformations that are only a couple of nanometers high. In order to image the protein, flat surfaces need to be used. Below is a modified procedure from Hegner *et al.*[15] which was used to obtain gold surfaces of RMS roughness less than 0.3 nm. These surfaces are stable for several months and contamination is minimal since the gold substrate is only exposed right before submerging into the appropriate solvent.

Mica discs are cleaved and heated for approximately 3 hours at 300 °C in a Ladd Vacuum Evaporator followed by gold (99.95%) deposition onto their surface. Surfaces are then inverted onto glass coverslips using EPO-TEK 377 in a 1:1 mass ratio, and placed in an oven at 150°C for ~ 1.5 hours. Gold substrates can be obtained by mechanically removing the mica with tweezers. Organic solvents such as tetrahydrofuran (THF) can also be used to separate the mica from the gold; however, chemical removal of the gold can result in pitting and time frames for removal of the gold can easily last over an hour. Any remaining mica islands on the gold surface can then be detected using conductivity measurements. The surfaces obtained from this procedure have

an RMS roughness of 0.3 nm or less, and it allows the gold surfaces to be prepared and stored for weeks before running an experiment without contamination of the surface.

BIBLIOGRAPHY

1.   Florin, E.; Moy, V.T.; Gaub, H.E. *Science*. **1994**, 264, 415.

2.   Bemis, J.; Akhremitchev, B.; Walker, G. *Langmuir*. **1999**, 15, 2799.

3.   Smith, B.L.; Schaeffer, T.E.; Viani, M.; Thompson, J.B.; Frederick, N.A.; Kindt, J.; Belcher, A.; Stucky, G.D.; Morse, D.E.; Hansma, P.K. *Nature* **1999**, 399, 761.

4.   Zhang, W.K.; Zou, S.; Wang, C.; Zhang, X.J. *J. Phys. Chem. B* **2000**, 104, 10258.

5.   Al-Maawali, S.; Bemis, J.E.; Akhremitchev, B.B.; Leecharoen, R.; Janesko, B.G.; Walker, G.C. *J. Phys. Chem. B*. **2001**, 105, 3965.

6.   Ortiz, C.; Hadziioannou, G. *Macromolecules*. **1999**, 32, 780.

7.   Tivanski, A.V.; Bemis, J.E.; Akhremitchev, B.B.; Liu, H.; Walker, G.C. *Langmuir*. **2003**, 19, 1929.

8.   Strunz, T.; Oroszlan, K.; Schafer, R.; Guntherodt, H. *Proc. Natl. Acad. Sci*. **1999**, 96, 11277.

9.   Liphardt, J.; Onoa, B.; Smith, S.B.; Tinoco Jr., I.; Bustamante, C. *Science*. **2001**, 292, 733.

10.   Kellermayer, M.S.Z.; Smith, S.B.; Bustamante, C.; Granzier, H.L. *Biophys. J*. **2001**, 80, 852.

11.   Tskhovrebova, L.; Trinick, J.; Sleep, J.A.; Simmons, R.M. *Nature*. **1997**, 387, 308.

12.   Rief, M.; Gautel, M.; Oesterhelt, F.; Fernandez, J.M.; Gaub, H.E. *Science*. **1997**, 276, 1109.

13.   Oberhauser, A.F.; Marszalek, P.E.; Erickson, H.P.; Fernandez, J.M. *Nature*. **1998**, 393, 181.

14.   Law, R.; Carl, P.; Harper, S.; Dalhaimer, S.; Speicher, D.W.; Discher, D.E. *Biophys. J.* **2003**, 84, 533.

15.   Hegner, M.; Wagner, P.; Semenza, G. *Surf. Sci.* **1993**, *291*, 39.

2. SINGLE-MOLECULE FORCE SPECTROSCOPY OF ISOLATED AND AGGREGATED FIBRONECTIN PROTEINS ON NEGATIVELY CHARGED SURFACES IN AQUEOUS LIQUIDS[1]

Plasma fibronectin (FN) was adsorbed to negatively charged surfaces, and the mechanical behavior of both isolated and aggregated FN molecules was observed using molecular force spectroscopy. Images of FN molecules show that the isolated proteins are already partially denatured and mechanically pulling on them yields force transitions at distance intervals significantly shorter than the domains' contour lengths. Only when FN was aggregated on the surface did force transitions occur at length intervals corresponding to Type III domain lengths. Apparently, FN's density on the surface plays a critical role in protein stabilization. The dependence of the transition forces on the loading rates was also measured and modeled. In measurements done on single proteins in aggregates, one barrier in the direction of the applied force was observed which arose from domain denaturation; however, studies of isolated, single molecules revealed two barriers, where both arise from protein-surface interactions.

---

[1] Reproduced with permission from Meadows, P. Y.; Bemis, J. E.; Walker, G. C. *Langmuir*, **2003**, 19, 9566-9572, Copyright 2003, American Chemical Society.

2.1. INTRODUCTION

When a surface is exposed to an aqueous solution of protein, it typically becomes covered by a proteinaceous film. For cardiovascular implants, protein deposition can then lead to adverse responses within the host. These include, but are not limited to, cellular adhesion, activation, and formation of thrombi which can then detach forming possibly life-threatening emboli.[1,2] To eliminate or minimize thrombogenesis on implant materials and other protein deposition effects, many groups have begun to explore the mechanism behind protein adsorption.[3-8] Changes in the state of hydration of both the substrate and the protein as well as rearrangement of the protein's structure and redistribution of its charged groups are a few of the factors involved in protein adsorption.[3-8] In addition to these intermolecular forces, surface chemistry,[9-15] topography,[15-17] protein concentration, solvent viscosity, and ionic strength[18] have also been found to play critical roles in regulating protein and cellular adhesion. In the work presented here, we examine the mechanical behavior of an adhesion promoting protein physisorbed to negatively charged surfaces using an atomic force microscope (AFM).

AFM has become a widely used tool for measuring inter- and intramolecular interactions: ligand-receptor adhesion forces,[19] polymer elasticity[20-24] and conductivity,[25] DNA[26] and RNA[27] folding kinetics, and the elastic properties of proteins in the extracellular matrix.[28-32] Here, we use an AFM as a single molecule force probe to study the mechanical properties of fibronectin at negatively charged surfaces. The basic methodology behind an AFM and the interpretation of the data collected will not be discussed here because of the extensive work already reported in literature.[33-39]

Fibronectin was chosen as the focus of this study because of its ability to bind numerous molecules such as heparin, fibrin, and collagen, but in particular, because of its role in mediating

cellular adhesion to surfaces within the bloodstream and extracellular matrix.[40,41] Fibronectin is a 450kDa glycoprotein that is composed of two nearly identical polypeptide chains linked near their carboxyl termini *via* two disulfide bonds. Each monomer is composed of twelve Type I, two Type II, and seventeen Type III domains.[40,41] Both Type I and Type II domains possess disulfide bonds whose strength precludes their mechanical denaturation in the force-extension experiments reported here; however, Type III domains which lack disulfide bonds can be mechanically denatured, and it is also these domains which are responsible for cellular binding.

We found that the density of protein adsorption plays a significant role in enabling domain denaturation by force spectroscopy. In the experiment, the protein was adsorbed to a surface; the tip was brought into contact with the protein and pulled away from the substrate, extending the protein between the tip and the surface. When FN was isolated on the surface, the transitions observed in the force *versus* distance data occurred at lengths and with forces uncharacteristic of Type III domain unfolding events, suggesting the proteins were already pre-denatured on the surface. Only when the proteins were aggregated on the surface were force transitions observed at distance intervals characteristic of domain denaturation. Apparently, FN is stabilized by the presence of neighboring molecules which prevents its surface denaturation. A loading rate analysis confirmed this as well. These plots suggest that the short lengths and small rupture forces observed were most likely due to a specific surface-protein interaction.

2.2. EXPERIMENTAL DETAILS

2.2.1. General

All glassware and glass substrates (Ted Pella, Inc., Redding, CA) were soaked overnight in a base bath containing 500g KOH (J.T. Baker (Scientific Equipment Company), Aston, PA), 500ml of tap water, and 4L of iso-Propanol (VWR International, Inc., Bridgeport, NJ). Water used in these experiments was purified to 18MΩ·cm resistivity using a Barnstead NANO pure filter.

2.2.2. Solution Preparation

Bovine fibronectin from plasma (Sigma, St. Louis, MO) was used to prepare a 20μg/ml solution in phosphate buffered saline (PBS: 10mM Na_2HPO_4 (J.T. Baker), 138mM NaCl (Sigma), and 2.7mM KCl (Mallinckrodt, Phillipsburg, NJ)) with 1% NaN_3 (Sigma). The solution was stored at 4ºC. 1M and 4M guanidinium hydrochloride (GdmHCl) solutions (Sigma) were also prepared for experiments involving denaturation by added salt.

2.2.3. Sample Preparation

Mica (SPI, West Chester, PA) was attached *via* epoxy to a glass microscope slide (VMR Scientific, Inc., West Chester, PA). 45μl of 1 μg/ml FN solution was deposited on a freshly cleaved mica surface for five minutes, followed by gentle rinsing of the surface with 3ml of water. The surface was then dried using a strong flow of nitrogen before imaging in water, PBS,

or GdmHCl solutions. Experiments involving protein denaturation followed a similar procedure except the protein was denatured before exposed to the surface, and the denaturant was also used as the imaging solvent. To prepare aggregated protein samples, the surfaces were allowed to remain under a 20 μg/mL FN solution at 4°C for 18-24 hours before imaging in H_2O or PBS.

2.2.4. AFM Cantilevers

Olympus gold-coated cantilevers were purchased from Asylum Research (Santa Barbara, CA) and used as received from the company. Contact Si_3N_4 cantilevers from Digital Instruments-Veeco Metrology (Santa Barbara, CA) were allowed to soak for 1.5 hours in a 1:10 (v/v) solution of diluted $HF:H_2O$.[42] Spring constants ranged from 30pN/nm to 70pN/nm and were determined using the thermal noise method.

2.2.5. AFM Measurements/Analysis

All measurements were obtained using molecular force probes from Asylum Research which were capable of moving a cantilever in one dimension (MFP-1D) or in three dimensions for surface imaging (MFP-3D). The instruments were controlled with Igor Pro 4.01 (MFP-1D) or 4.05A (MFP-3D) (Wavemetrics, Lake Oswego, Oregon) with a modified version of the MFP software 1.30R1 (MFP-1D) or 0.9r1 (MFP-3D). For the MFP-3D measurements, the tip was brought within 10 microns of the surface, and the system was allowed to thermally equilibrate for at least 2 hours before data collection. Images were obtained in an intermittent contact mode using a gold-coated cantilever with a tip oscillation of 60-70nm. All force-extension curves were

collected at a piezo velocity of 2 μm/sec. Data analysis was performed using software written in Matlab (Math Works, Inc., Natick, MA).

2.3. RESULTS AND DISCUSSION

2.3.1. Mechanical Behavior of Single Molecules of FN on a Mica Substrate

Images of the prepared samples were collected followed by molecular pulling experiments in region-specific surface areas. Figure 6 shows two images collected underwater, one of a control surface and one of FN deposited for five minutes. As can be seen, FN adopts a compact conformation in this solvent. Lin *et al.*[43] have observed FN in a more extended conformation when adsorbed to mica but in the absence of solvent. Under these same conditions, we too have observed a less compact structure; however, in water, FN became more compact, appearing to redistribute its charged groups. Phosphate buffered saline, although resembling physiological conditions, could not be used in these studies since protein desorption prevailed. Tip contamination under these buffered conditions was often observed as well.

Before conducting the molecular pulling experiments, it was necessary to confirm that the larger objects seen in Figure 6 were indeed single FN molecules rather than aggregates since smaller objects were also observed on the substrate. In a rough approximation, the minimum height required for a single FN molecule to adopt a spherical conformation was calculated to be 10nm. This estimate indicates that the larger objects seen in Figure 6 are not aggregates but single molecules of FN which were then chosen for the pulling experiments. Thus, immersion

of the substrate in a protein solution with a concentration of 1µg/ml for five minutes was sufficient to obtain numerous, but isolated protein molecules on the surface.
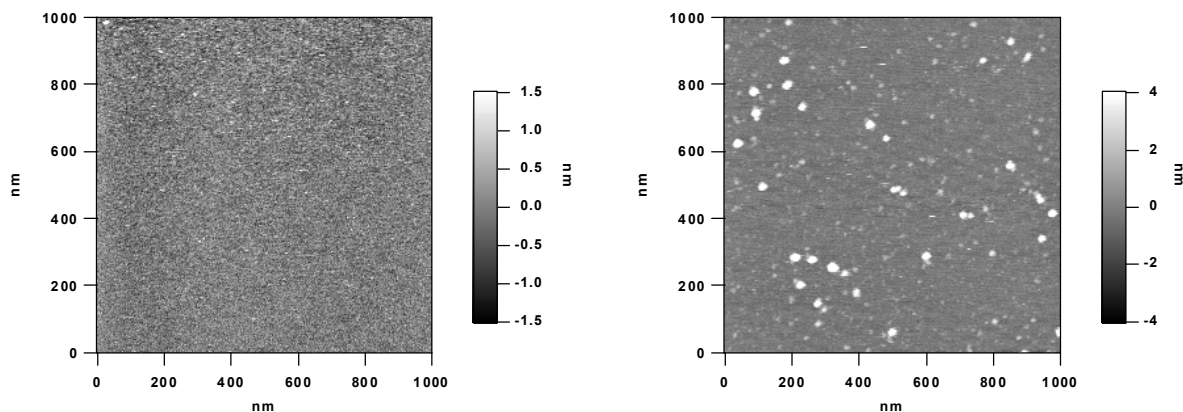
Figure 6 Two images showing before (left) and after (right) sparse protein deposition on mica. The larger molecules in the right image are single molecules of FN. The smaller objects are probably protein fragments. As can be seen in the height scale, the isolated proteins are greater than 8nm in height.

A number of steps were taken to ensure that single molecule experiments were accomplished using only uncontaminated tips. First, images were collected in an intermittent contact mode followed by force-extension plots on *selected* regions of the surface which provided a great advantage over random sampling of the surface area. Selecting the molecule to pull helped to ensure that only, isolated, single molecules on the surface were probed. The proteins were also imaged on the surface before and after pulling, indicating that the proteins remained on the substrate. Further confirmation that the tip had not become contaminated was obtained by collecting force plots on bare regions of the substrate after protein probing. Less than 0.1% of the force plots showed stretching events which makes it unlikely that the tip in previous force plots had been fouled with protein. High-resolution topographic imaging was also done after the pulling experiments; these images cannot be obtained if the tip has become fouled

with protein. Thus, the combination of imaging with spatially specific pulling measurements gave great confidence that the data obtained was due to the mechanical stretching of a single, isolated FN molecule that remained adhered to the substrate.

Table 1 summarizes the data collected in one of the imaging and protein pulling experiments. The surface bound protein physisorbed to the tip in approximately 18% of the force plots, and in almost half of these occurrences only one force transition resulted, indicative of protein-tip rupture. The remaining force-distance curves, which showed multiple ruptures, were analyzed for their relation to protein dynamics. Figure 7 displays a force plot containing two relevant force transitions as well as a plot of the difference in length (ΔL) between successive ruptures. This length was calculated using the points of the cantilever's maximum extension. A most probable length of 9.2 ± 0.4nm was observed when all transition lengths were included in the fitted distribution, and a most probable length of 9.5 ± 0.5nm was observed when the last transition length (gap between the second to last and last rupture) was excluded in the distribution (as shown in Figure 7). These lengths do not correlate with the values reported in literature (25.1 ± 0.5nm[44] or 28.5 ± 4.0nm)[45] for Type III domain denaturation events in the protein tenascin[45] or for 0.2mg/ml of FN adsorbed on a Petri dish.[44] However, Oberhauser *et al*.[46] did observe a peak at 9.3 ± 1.6nm when pulling a polyprotein containing the first Type III domain. Although this represented the minority of their data, this length clearly dominates the results reported here, as seen in Figure 7.

Table 1 Summary of a Typical Force Spectroscopy Experiment on Single Molecules Collected in Water on a Mica Substrate*

Breakdown of Force Plots Collected	Number
Force Plots Collected	12,133
Force Plots Where FN is Contacted	10,853
Force Plots Where FN is Contacted and Adsorbs	1,908
Single Rupture Force Plots	877
Multiple Rupture Force Plots Used for Analysis • Total Number of Ruptures Used in These Plots	853[*] 2,679

*Force plots with rupture forces near the limit of our resolution were excluded.
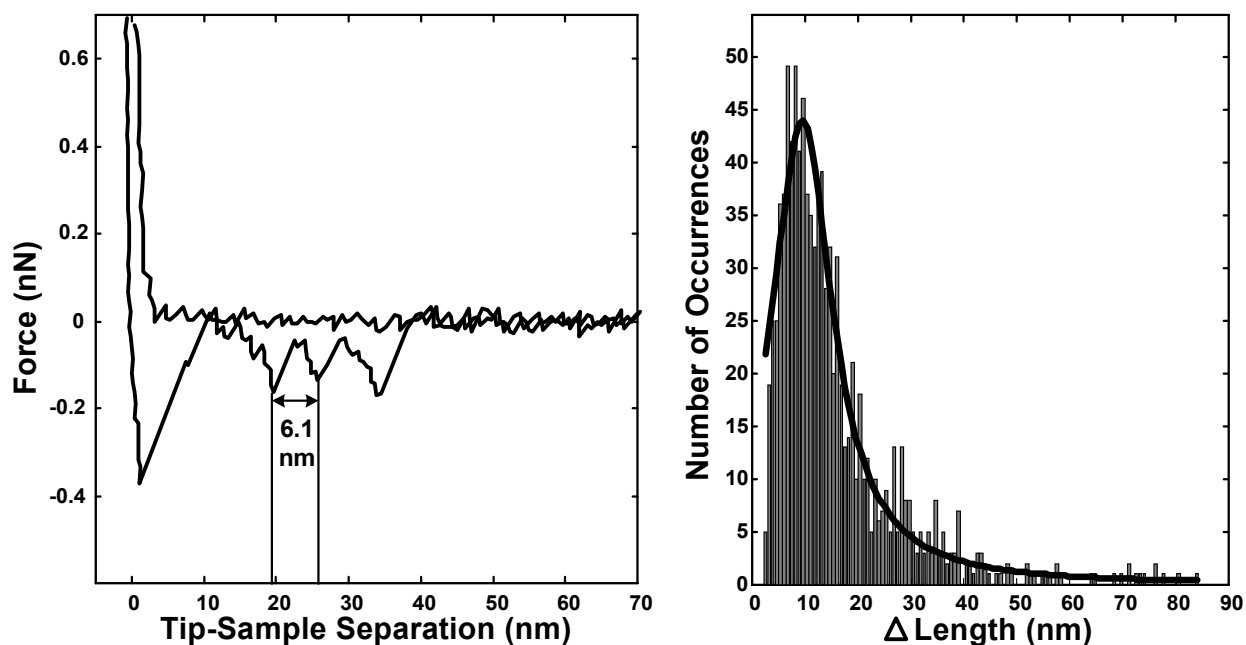
Figure 7 The left panel shows a force plot obtained when extending single molecules of FN away from a mica surface in water. The length intervals between successive ruptures was determined by subtracting the difference in tip-sample separations at points prior to the cantilever returning to near zero force, as illustrated by the vertical lines. The right panel gives a histogram of these length intervals; the most probable value of 9.5 ± 0.5nm was determined by a Lorentzian fit to the data.

Possible explanations for this short length could be the result of interdomain interactions, domain intermediates, or a specific surface-protein interaction. To examine the potential role of interdomain interactions, a 1M GdmHCl solution was used to minimize these forces.[47] In these denaturing solutions, more extended protein conformations were observed in the surface images (data not shown), confirming these interactions had been reduced; however, the most probable length interval obtained was ~14nm. This slightly longer length interval is consistent with the denaturant partly extending the protein on the surface, but it is still shorter than what would be expected for entire domain unfolding.

An unfolding intermediate could also generate the 9.5nm length interval. Several steered molecular dynamics simulations (SMD) have been performed on FN; Gao et al.[48] have shown an intermediate at 10nm which occurs when the A and B-strands of the tenth Type III domain unravel prior to the interstrand hydrogen bonds breaking between the F and G-strands. Oberhauser et al.[46] assigned this phenomenon to the 9.3nm transition length they observed in the polypeptide containing the first Type III domain. To determine if the short length observed in this work was indeed a result of an intermediate, FN was denatured using 4M GdmHCl, a concentration documented to denature the entire protein in solution.[47] Unfortunately, with this high concentration, salt deposition prevented successful pulling experiments. Thus, an intermediate contributing to the 9.5nm length interval has not been excluded, but as will be discussed next, force plots illustrating this length interval indicate the forced separation of the protein from the surface.

2.3.2. Mechanical Behavior of FN Aggregates

Because extending isolated single molecules of FN did not produce force transitions at length intervals previously associated with Type III domain unfolding events, we explored the possibility that the protein had undergone partial surface denaturation. Several groups[4-5,13,49] have observed that low-density protein coverage results in a conformationally inactive protein and only at a higher coverage does the protein become stable. Neighboring proteins thus prevent domain denaturation[13] at the surface, perhaps by protecting the domains from interacting with the surface. Figure 8 reveals a force plot obtained for samples of densely deposited FN as well as a histogram of ΔL for these regular, repeating microruptures. The peak shifts from 9.5 ± 0.5 nm to 26.2 ± 0.6nm, a length interval agreeing quite well with literature reports for domain unfolding events. When varying environmental factors such as solvent, substrate, and tip material, negligible differences in the length were observed for densely covered surfaces; the domain unfolding events were always present but the rupture forces did vary. Table 2 summarizes the results for all experiments conducted. In general, higher rupture forces were obtained with a gold-coated tip than with a silicon nitride cantilever, and as expected the rupture forces in a denaturant were smaller. Furthermore, the rupture transition forces in the single molecule studies were smaller than those observed in the aggregate studies that probed domain unfolding events.
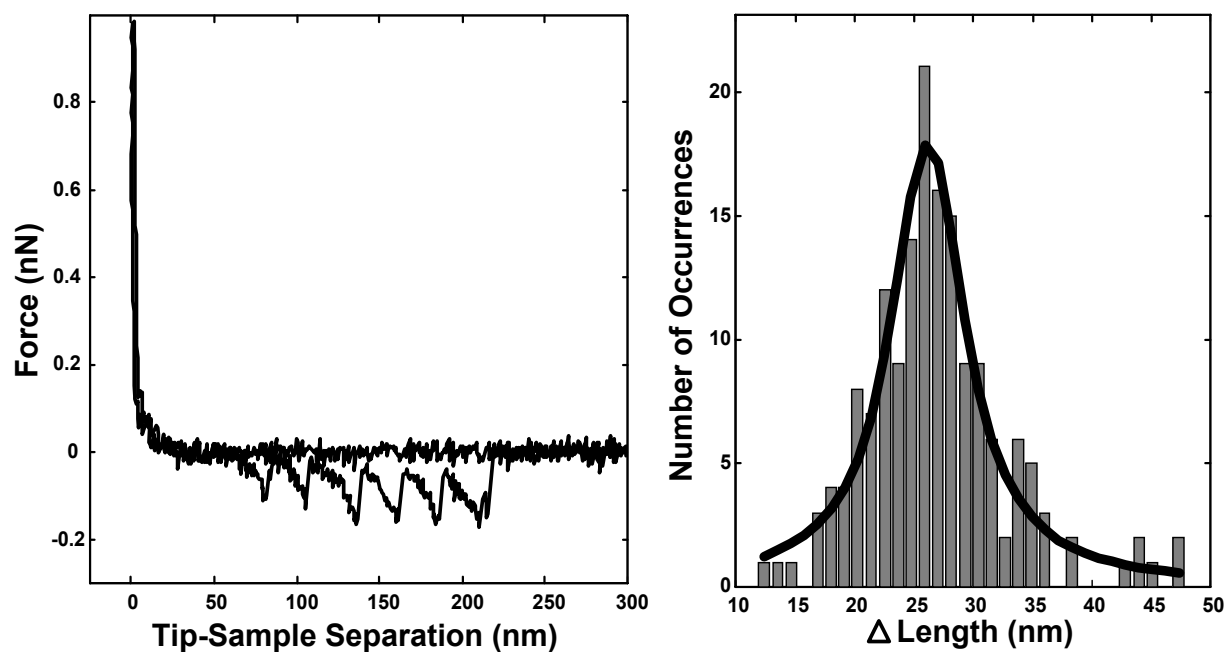
Figure 8 The left panel shows a force plot obtained when extending molecules in aggregates of FN from mica. A histogram of the difference in length between successive ruptures is seen on the right. The Lorentzian fit of the data shows a length of approximately 26.2 ± 0.6nm. This length is similar to the length interval reported in literature[44-45] where it was ascribed to the unfolding of a Type III domain. It is important to point out that when the protein is aggregated, the force plots often show complex intermolecular interactions in addition to these equally spaced microruptures.

Table 2 Summary of the Rupture Forces and Difference in Length Between Successive Ruptures

Experimental Conditions	ΔLength (nm)*	Rupture Force (pN)
Mica/Au tip/water/isolated single molecules	9.2 ± 0.4	113.5 ± 2.6
Mica/Au tip/1M GdmHCl/isolated single molecules	14.5 ± 1.3	80.8 ± 2.9
Mica/Au tip/water/dense FN coverage	26.2 ± 0.6	170.2 ± 4.2
Mica/Au tip/PBS/dense FN coverage	27.1 ± 0.3	166.3 ± 2.5
Glass/Au tip/water/dense FN coverage	26.2 ± 0.6	204.0 ± 3.2
Glass/Au tip/PBS/dense FN coverage	26.8 ± 0.4	154.1 ± 1.9
Glass/Si$_3$N$_4$/PBS/dense FN coverage	25.7 ± 0.3	125.4 ± 1.1

*Values from the ΔLength distributions include the last rupture within a force plot unlike the values reported here for the force distribution plots.

2.3.3. Transition State Crossing Under Applied Force

To gain insight into the energy landscape traversed during forced extension of proteins, the relationship between the transition (rupture) force and the rate at which the force was applied to the system was explored. Based on the work from Bell and Evans,[50-56] an exponential relationship exists between the rate of dissociation (k_{off}) of a ligand-receptor complex and the externally applied force F (equation1).

$$k_{off}(F) = k_{off}(0)e^{Fx_\beta / k_B T}$$ (1)

Here k_BT represents the thermal energy, $k_{off}(0)$ is the rate of dissociation under zero applied force, and x_β is the distance from the free energy minimum to the transition state from the ground state projected along the direction of applied force. Because force is applied along a distance x, the free energy for dissociation decreases linearly with the applied force (equation 2).

$$\Delta G^{\#}(F) = \Delta G^{\#}(0) - Fx_\beta \tag{2}$$

As this force is applied to a system, the observed unbinding force will depend on the rate at which the force is applied to the system, *i.e.* the loading rate. As equation 3 illustrates, there is a logarithmic dependence of this dissociation force (F) on the loading rate (r).[51-58]

$$F = \frac{k_BT}{x_\beta} \ln\left(\frac{x_\beta r}{k_{off}^o k_B T}\right) \tag{3}$$

Over several orders of magnitude, a plot of rupture force *versus* ln(r) will reveal linear regions of increasing slope, each region corresponding to a barrier traversed along the direction of applied force. Using equation 3 then allows x_β to be determined and extrapolating back to zero applied force, $k_{off}(0)$ and $\Delta G^{\#}(0)$ can be determined through equations 4 and 5, where h is Planck's constant.

$$k_{off}(0) = \frac{r \cdot x_\beta}{k_B T} \tag{4}$$

$$k_{off}(0) = \frac{k_B T}{h} e^{-\Delta G^{\#}/k_B T} \tag{5}$$

Thus from a loading rate plot, the thermodynamic parameters involved in ligand-receptor dissociation *via* AFM can be approximated.

However, as pointed out by Evans, unlike a ligand-receptor scenario which displays linear elastic properties, application of force on proteins or highly flexible polymers results in nonlinear elastic stretches. The model described briefly above works well for the first example,

yet complications can arise for the latter case,[51,54] when determining the rupture force dependence on loading rate. Nevertheless, Rief[30] and Carrion-Vasquez[59] have observed a linear dependence of unbinding force *versus* the logarithm of the loading rate when mechanically unfolding proteins. Therefore, this model will be applied here to determine the thermodynamic parameters associated with forced unfolding.

In the data presented below, the rupture force was determined from the force plots using the data point just prior to where the cantilever returns to its rest position, *i.e.* the point of maximum extension of the cantilever. Loading rate (r) was also determined directly from the force plots through equation 6

$$r_{rupture} = \frac{\Delta F}{\left(\dfrac{n+1}{S_{rate}}\right)} \tag{6}$$

where n is one less than the number of points used to obtain ΔF, S_{rate} is the sampling rate in the data acquisition in points per second, and ΔF is the change in the attractive force from the point of rupture to five points previous to the rupture.

Figure 9 shows three loading rate plots that were obtained while Table 3 gives the corresponding parameters using the mean values for force and loading rate. In the analysis, represented by Panels A and B, the last rupture in the force plots was omitted to exclude the process of the protein breaking free from the tip. As can be seen in Figure 9B, the regular repeating ruptures observed in Figure 8 of the protein aggregate studies produced only one linear region in the loading rate plot. However, the isolated single studies showed two linear regions. Using k_BT/h as the pre-exponential factor in the unfolding rate expression gives an acceptable value for the barrier position in the shallow sloped region in Figure 9A but an unphysical barrier position (~0.02nm) for the steeper linear region of the data. Furthermore, in agreement with our

previous conclusions, Table 3 also reveals that a higher surface density of proteins provides

added kinetic stability.
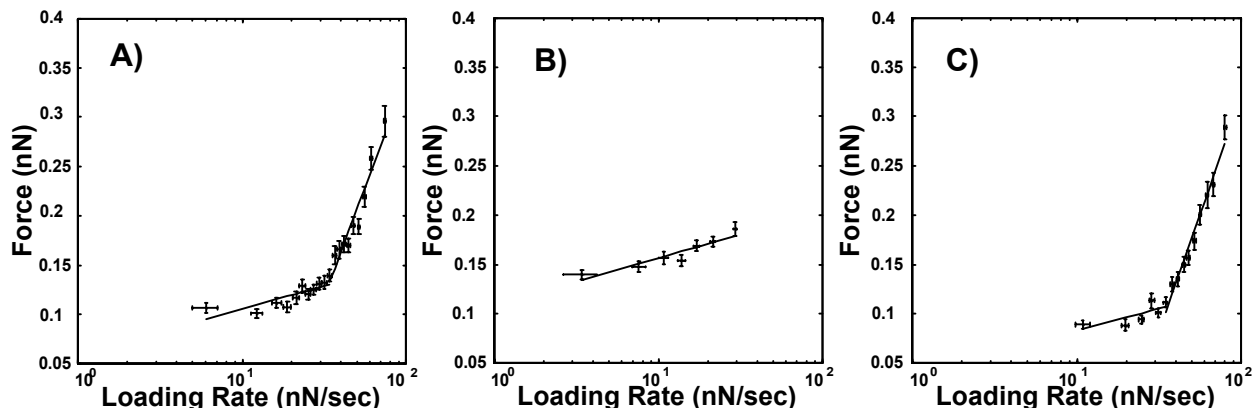
Figure 9 Plots illustrating the relationship between rupture force and loading rate. The binned points represent the mean values of the force and loading rate while the error bars correspond to the standard deviation of the mean. Plot A corresponds to measurements performed on single FN molecules isolated on a mica substrate in water. Plot B represents FN densely deposited on a glass substrate in PBS. In both of these plots, the last rupture in the force plots, which corresponds to rupture of the protein from the tip, is excluded from the analysis. In Plot C, rupture forces in plots with only one pulling event are analyzed for isolated single FN molecules on mica in water, which therefore includes the protein-tip rupture. Under the Bell model and its extensions, each linear region corresponds to a barrier crossing process in the forced extension of the protein between the tip and the substrate. The shallow sloped regions correspond to transitions between protein states that occur *via* rate processes that are plausible when modeled with a pre-exponential factor of k_BT/h. The sloped feature in Panel B implies reaction coordinate parameters similar to those previously observed by Oberhauser *et al.*[46]. The steeper, second linear regions in Plots A and C yield a non-physical barrier position if k_BT/h is used as the pre-exponential factor in the rate expression, and it is probable that frictions along these barrier crossings are much greater than observed in panel B. Such larger friction is probably due to damped dynamics of protein bound to the substrate in A and the tip in C.

Table 3 Unfolding Barrier Positions and Energies

Experimental Conditions	x_{beta} (nm)	$\Delta G(0)$ (kcal/mol)
Mica/Au tip/water/isolated single molecules	0.20 ± 0.05	16.8 ± 0.60
	$0.021 \pm 2.0 \cdot 10^{-3}$	14.7 ± 0.28
Mica/Au tip/1M GdmHCl/isolated single molecules	0.19 ± 0.06	16.4 ± 0.66
	$0.013 \pm 7.0 \cdot 10^{-4}$	15.0 ± 0.15
Mica/Au tip/water/dense FN coverage	0.19 ± 0.07	18.2 ± 1.3
Mica/Au tip/PBS/dense FN coverage	0.24 ± 0.06	19.0 ± 1.2
Glass/Au tip/water/dense FN coverage	0.25 ± 0.05	20.1 ± 1.1
Glass/Au tip/PBS/dense FN coverage	0.20 ± 0.03	18.0 ± 0.57
Glass/Si$_3$N$_4$/PBS/dense FN coverage	0.28 ± 0.06	18.9 ± 0.87
Mica/Au tip/water/isolated single molecules *Only single-rupture plots*	0.21 ± 0.095	16.2 ± 1.0
	$0.020 \pm 1.2 \cdot 10^{-3}$	14.6 ± 0.18

Above it was suggested that either a substructure of a domain or a specific surface-protein interaction could give rise to the uncharacteristic force and ΔL values that were obtained. To test for a surface-protein interaction, the rupture forces from force plots displaying only one stretching event, indicative of protein-tip rupture, were plotted as a function of loading rate (Figure 9C). As can be seen in this Panel, two linear regions were found with distances to the barriers being similar to those found in the single molecule studies. Therefore, since the last rupture had been removed from the analysis in Panels A and B of Figure 9, and Panel C reveals a specific surface-protein interaction involving two barriers, we conclude that a protein-surface

interaction is indeed occurring in the isolated, single molecule studies and is apparently the dominant state.

Because the second linear region seen in Figure 9A could be fit by the model but the distance to the barrier is unphysical, an alternative model is needed. A more realistic barrier position (a few bond lengths) might be obtained if it is assumed that the direction of the applied force is at a considerable angle to the initial direction for the surface dissociation, but the validity of this assumption and the other assumptions of equation (3) along with the role of internal friction of the protein need to be investigated further.[60-66]

2.4. CONCLUSIONS

The mechanical behavior of FN molecules that are elongated between an AFM tip and a negatively charged substrate were measured and analyzed. Several solvents, substrates, and tip materials were tested. Plots of distributions of rupture force and the lengths between successive ruptures were measured. Type III domain unfolding events were not predominant when pulling single, isolated molecules on mica. Apparently the proteins, where isolated from each other, became unstable, and underwent partial denaturation at the surface prior to their extension. This would explain the absence of a strong peak at ~25nm, the length observed for mechanically unfolding a Type III domain. When the protein's concentration on the surface was increased to the point of surface aggregation, Type III domain denaturation was observed to occur in our extension measurements. This implies that the proteins exposed on the surface did not undergo surface denaturation before elongating with an AFM tip. This finding that protein density enhances protein stability agrees well with other groups' work in unrelated experiments.[4-5, 13, 49]

For example, using circular dichroism, Norde and Favier[4] measured the structural rearrangements of bovine serum albumin and hen's egg lysozyme on silica particles. For both proteins, they observed a decrease in the α-helix content upon adsorption implying surface denaturation, but this effect diminished upon increasing the protein's surface coverage. Furthermore, in the study by Grinnell and Feld,[13] they observed the adsorption characteristics of plasma FN on nonwettable bacteriological dishes. They concluded that at a low surface concentration, FN was unfolded into an inactive conformation, but at a higher surface concentration, the molecular packing requirements prevented unfolding. Therefore, our results from an AFM prove to be consistent with other groups' work; however, our technique allows us to observe the behavior of a single molecule and can provide additional information such as the details of the unfolding thermodynamics. Our results could also provide insight that might be important for designing biocompatible substrates suitable for cellular seeding. As recently reviewed by Mrksich[67] and reported in a research article by Garcia *et al.*[68], it was found that different surfaces induce protein conformations that elicit a variety of responses to antibody binding and cellular growth. For example, binding of HFN7.1, an antibody, to fibronectin on uncharged polystyrene has a FN surface concentration dependence that indicates protein-protein interactions initially enhance antibody binding.[68] The relation between the concentration dependence we found and its influence on cellular response deserves further investigation.

We also found that the most probable force transition events occurring in our single molecule studies results from a protein-surface interaction. In the aggregate studies, the microruptures for domain unfolding events produced only one linear region in a loading rate plot where the single molecule studies produced two. Loading rate plots of force plots containing only a single rupture, which most likely probe a specific surface-protein interaction, gave rise to

two linear regions with parameters very similar to the single molecule studies. Combining the results of ΔL, rupture force, loading rate plots, and the thermodynamic parameters obtained from this analysis, it is concluded that when pulling single, isolated molecules of fibronectin on mica, domain denaturation is not observed. Apparently the protein is already partially denatured.

BIBLIOGRAPHY

1. Haycox, C.L.; Ratner, B.D. *J. Biomed. Mater. Res*. **1993**, 27, 1181.

2. Bruck, S.D. *Biomaterials, Medical Devices and Artificial Organs*. **1983-84**, 11, 271.

3. Hlady, V.; Buijs, J. *Curr. Opin. Biotech*.   **1996**, 7, 72.

4. Norde, W.; Favier, J.P. *Colloids Surfaces*. **1992**, 64, 87.

5. Brash, J.L.; Horbett, T.A., Eds. *Proteins at Interfaces II: Fundamentals and Applications*. American Chemical Society: Washington, DC, 1995.

6. Haynes, C.A.; Norde, W. *Colloid Surface B*. **1994**, 2, 517.

7. Norde, W. *Adv. Colloid Interf. Sci*. **1986**, 25, 267.

8. Haynes, C.A.; Norde, W. *J. Colloid Interface Sci*. **1995**, 169, 313.

9. Lestelius, M.; Liedberg, B.; Tengvall, P. *Langmuir*. **1997**, 13, 5900.

10. Scotchford, C.A.; Gilmore, C.P.; Cooper, E.; Leggett, G.J.; Downes, S. *J. Biomed. Mater. Res*. **2002**, 59, 84.

11. Sigal, G.B.; Mrksich, M.; Whitesides, G.M. *J. Am. Chem. Soc*. **1998**, 120, 3464.

12. Mrksich, M. *Cell. Mol. Life Sci*. **1998**, 54, 653.

13. Grinnell, F.; Feld, M.K. *J. Biomed. Mater. Res*. **1981**, 15, 363.

14. Kidoaki, S.; Matsuda, T. *Langmuir*. **1999**, 15, 7639.

15. Denis, F.A.; Hanarp, P.; Sutherland, D.S.; Gold, J.; Mustin, C.; Rouxhet, P.G.; Dufrene, Y.F. *Langmuir*. **2002**, 18, 819.

16. McFarland, C.D.; Thomas, C.H.; DeFilippis, C.; Steele, J.G.; Healy, K.E. *J. Biomed. Mater. Res*. **2000**, 49, 200.

17. Dufrene, Y.F.; Marchal, T.G.; Rouxhet, P.G. *Langmuir*. **1999**, 15, 2871.

18. Tripp, B.C.; Magda, J.J.; Andrade, J.D. *J. Colloid Interface Sci*. **1995**, 173, 16.

19. Florin, E.; Moy, V.T.; Gaub, H.E. *Science*. **1994**, 264, 415.

20. Bemis, J.; Akhremitchev, B.; Walker, G. *Langmuir*. **1999**, 15, 2799.

21. Smith, B.L.; Schaeffer, T.E.; Viani, M.; Thompson, J.B.; Frederick, N.A.; Kindt, J.; Belcher, A.; Stucky, G.D.; Morse, D.E.; Hansma, P.K. *Nature* **1999**, 399, 761.

22. Zhang, W.K.; Zou, S.; Wang, C.; Zhang, X.J. *J. Phys. Chem. B* **2000**, 104, 10258.

23. Al-Maawali, S.; Bemis, J.E.; Akhremitchev, B.B.; Leecharoen, R.; Janesko, B.G.; Walker, G.C. *J. Phys. Chem. B*. **2001**, 105, 3965.

24. Ortiz, C.; Hadziioannou, G. *Macromolecules*. **1999**, 32, 780.

25. Tivanski, A.V.; Bemis, J.E.; Akhremitchev, B.B.; Liu, H.; Walker, G.C. *Langmuir*. **2003**, 19, 1929.

26. Strunz, T.; Oroszlan, K.; Schafer, R.; Guntherodt, H. *Proc. Natl. Acad. Sci*. **1999**, 96, 11277.

27. Liphardt, J.; Onoa, B.; Smith, S.B.; Tinoco Jr., I.; Bustamante, C. *Science*. **2001**, 292, 733.

28. Kellermayer, M.S.Z.; Smith, S.B.; Bustamante, C.; Granzier, H.L. *Biophys. J*. **2001**, 80, 852.

29. Tskhovrebova, L.; Trinick, J.; Sleep, J.A.; Simmons, R.M. *Nature*. **1997**, 387, 308.

30. Rief, M.; Gautel, M.; Oesterhelt, F.; Fernandez, J.M.; Gaub, H.E. *Science*. **1997**, 276, 1109.

31. Oberhauser, A.F.; Marszalek, P.E.; Erickson, H.P.; Fernandez, J.M. *Nature*. **1998**, 393, 181.

32. Law, R.; Carl, P.; Harper, S.; Dalhaimer, S.; Speicher, D.W.; Discher, D.E. *Biophys. J* **2003**, 84, 533.

33. Zlatanova, J.; Lindsay, S.M.; Leuba, S.H. *Prog. Biophs. Mol. Bio*. **2000**, 74, 37.

34. Hugel, T.; Seitz, M. *Macromol. Rapid Comm*. **2001**, 22, 989.

35. Fisher, T.E.; Marszalek, P.E.; Oberhauser, A.F.; Carrion-Vazquez, M.; Fernandez, J.M. *J. Physiol*. **1999**, 520.1, 5.

36. Ludwig, M.; Rief, M.; Schmidt, L.; Li, H.; Oesterhelt, F.; Gautel, M.; Gaub, H.E. *Appl. Phys. A*. **1999**, 68, 173.

37. Willemsen, O.H.; Snel, M.M.E.; Cambi, A.; Greve, J.; De Grooth, B.G., Figdor, C.G. *Biophys. J*. **2000**, 79, 3267.

38. Fisher, T.E.; Oberhauser, A.F.; Carrion-Vazquez, M.; Marszalek, P.E.; Fernandez, J.M. *Trends Biochem. Sci.* **1999**, 24, 379.

39. Makarov, D.E.; Wang, Z.; Thompson, J.B.; Hansma, H.G. *J. Chem. Phys.* **2002**, 116(17), 7760.

40. McDonagh, J., Ed. *Plasma Fibronectin, Structure and Function*; Marcel Dekker: New York, 1985.

41. Mosher, D., Ed. *Biology of Extracellular Matrix: A Series Fibronectin*; Academic Press: San Diego, 1989.

42. Caution!! HF is a highly toxic solution and is extremely dangerous to work with; chemical resistant gloves, goggles, and an 8-inch minimum diameter face shield should be worn.

43. Lin, H.; Lal, R.; Clegg, D.O. *Biochemistry.* **2000**, 39, 3192.

44. Oberdorfer, Y.; Fuchs, H.; Janshoff, A. *Langmuir.* **2000**, 16, 9955.

45. Oberhauser, A.F.; Marszalek, P.E.; Erickson, H.P.; Fernandez, J.M. *Nature.* **1998**, 393, 181.

46. Oberhauser, A.F.; Badilla-Fernandez, C.; Carrion-Vazquez, M.; Fernandez, J.M. *J. Mol. Biol.* **2002**, 319, 433.

47. Khan, M.Y.; Medow, M.S.; Newman, S.A. *Biochem. J.* **1990**, 270, 33.

48. Gao, M.; Craig, D.; Vogel, V.; Schulten, K. *J. Mol. Biol.* **2002**, 323, 939.

49. Steadman, B.L.; Thompson, K.C.; Middaugh, C.R.; Matsuno, K.; Vrona, S.; Lawson, E.Q.; Lewis, R.V. *Biotechnol. Bioeng.* **1992**, 40, 8.

50. Bell, G.I. *Science.* **1978**, 200, 618.

51. Evans, E. *Annu. Rev. Biophys. Biomol. Struct.* **2001**, 30, 105.

52. Evans, E. *Faraday Discuss.* **1998**, 111, 1.

53. Evans, E.; Ludwig, F. *J. Phys.: Condens. Matter* **2000**, 12, A315.

54. Evans, E.; Ritchie, K. *Biophys. J.* **1999**, 76, 2439.

55. Merkel, R.; Nassoy, P.; Leung, A.; Ritchie, K.; Evans, E. *Nature* **1999**, 397, 50.

56. Evans, E.; Ritchie, K. *Biophys. J.* **1997**, 72, 1541.

57. Strunz, T.; Oroszlan, K.; Schumakovitch, I.; Guntherodt, H.-J; Hegner, M. *Biophys. J.* **2000**, 79, 1206.

58. Dettmann, W.; Grandbois, M.; Andre, S.; Benoit, M.; Wehle, A.K.; Kaltner, H.; Gabius, H.; Gaub, H.E. *Arch. Biochem. Biophys*. **2000**, 383, 157.

59. Carrion-Vasquez, M.; Oberhauser, A.F.; Fowler, S.B.; Marszalek, P.E.; Broedel, S.E.B.; Clarke, J.; Fernandez, J.M. *Proc. Natl. Acad. Sci*. **1999**, 96, 3694.

60. Sukhishvilli, S. A.; Chen, Y.; Mueller, J. D.; Gratton, E.; Schweizer, K. S.; Granick, S. *Nature* **2000,** 404, 146.

61. Jacob, M.; Schmid, F.X. *Biochemistry* **1999**, 38, 13773.

62. Swegat, W.; Schlitter, J.; Kruger, P.; Wollmer, A. *Biophys. J*. **2003**, 84, 1493.

63. Portman, J.J.; Takada, S.; Wolynes, P.G. *J. Chem. Phys*. **2001**, 114, 5082.

64. Plaxco, K.W.; Baker, D. *Proc. Natl. Acad. Sci*. **1998**, 95, 13591.

65. Alm, E.; Morozov, A.V.; Kortemme, T.; Baker, D. *J. Mol. Biol*. **2002**, 322, 463.

66. Ghatak, A.; Vorvolakos, K.; She, H.; Malotky, D.; Chaudhury, M.K. *J. Phys. Chem. B* **2000**, 104, 4018.

67. Mrksich, M. *Chem. Soc. Rev*. **2000**, 29, 267.

68. Garcia, A.J.; Vega, M.D.; Boettiger, D. *Mol. Biol. Cell* **1999**, 10, 785.

3. FORCE MICROSCOPY STUDIES OF FIBRONECTIN ADSORPTION AND SUBSEQUENT CELLULAR ADHESION TO SUBSTRATES WITH WELL-DEFINED SURFACE CHEMISTRIES[2]

Molecular force spectroscopy was used to study the mechanical behavior of plasma fibronectin (FN) on mica, gold, poly(ethylene) glycol (PEG), and -CH$_3$, -OH, and -COOH terminated alkanethiol self-assembled monolayers. Proteins were examined at two concentrations, one resulting in a saturated surface with multiple intermolecular interactions referred to as the aggregate state and another resulting in a semiaggregate state where the proteins were neither completely isolated nor completely aggregated. Modeling of the force-extension data using two different theories resulted in similar trends for the fitted thermodynamic parameters from which insight into the protein's binding state could be obtained. Aggregated proteins adsorbed on hydrophobic surfaces adopted more rigid conformations apparently as a result of increased surface denaturation and tighter binding while looser conformations were observed on more hydrophilic surfaces. Studies of FN in a semiaggregate state showed heterogeneity in the model's thermodynamic parameters suggesting that in the early stages of nonspecific adsorption, multiple protein conformations exist, each having bound irreversibly to the substrate. Proteins in this state all demonstrated a more rigid conformation than in the corresponding aggregate studies due to the greater number of substrate contacts available to the protein. Finally, the force spectroscopy experiments were examined for any biocompatibility correlation by seeding

---

substrates with human umbilical vascular endothelial cells. As predicted from the models used in this work, surfaces with aggregated FN promoted cellular deposition while surfaces with FN in a semiaggregate state appeared to hinder cellular deposition and growth. AFM's use as a means for projecting surface biocompatibility, although requiring additional testing, does look promising.

3.1.   INTRODUCTION

Engineering biocompatible materials requires an understanding of protein adsorption and cell adhesion to synthetic surfaces.   A cell's ability to specifically adsorb to the underlying proteinaceous film is governed primarily by the protein's conformational state on the surface. Factors including protein density,[1-5] surface chemistry,[4,6-11] topography,[11-13] ionic strength, hydration state, and solvent viscosity[14] have been found to be responsible for influencing a protein's surface conformation. Difficulty though can arise in modeling protein adsorption to synthetic surfaces since many of these substrates lack surface homogeneity. Model surfaces such as self-assembled monolayers (SAMs) of alkanethiols on gold are now being used to investigate the effects of surface chemistry on protein adsorption because of their well-controlled surface properties.[15-18]

In the work presented here, FN is the focus of study because of its role in building up extracellular proteins responsible for cell adhesion, neurite growth, and tissue repair.[19-21] This 450 kDa glycoprotein is composed of nearly two identical polypeptide chains connected near their carboxy termini *via* two disulfide bonds.[22-23] In physiological solution, each dimer is approximately 70 nm in length and consists of three types of charged, globular modules, termed Type I, Type II, and Type III domains.[22-23] Because of these charged groups, more flexible and extended conformations have been found on hydrophilic surfaces[24-26] while more compact but stronger binding conformations are produced on hydrophobic substrates.[24-28]   Greater perturbation of FN's secondary structure is also observed on hydrophobic surfaces.[29-30]

A more quantitative picture of FN's surface binding properties can now be obtained from an atomic force microscope (AFM). Since its invention in the 1980s,[31] the AFM has been useful for understanding ligand-receptor adhesion forces,[32] polymer and protein elasticity,[33-42] and the folding kinetics of several biological molecules.[43-44] Recent developments in modeling protein studies from an AFM[45-54] give insight into the dynamics of protein folding if we assume the molecule's reaction coordinate under applied force is the favored pathway in the absence of the pulling stress. This then allows the intrinsic thermodynamic parameters of the system to be explored using an AFM. To our knowledge, this is the first paper to provide quantitative estimates of FN's reaction free energy surface as a function of surface chemistry and protein density.

In this study, we examine model surfaces with well-controlled surface properties and their effect on FN's adsorption, stability, and conformational state. Modeling of FN's mechanical unfolding as a function of surface density and substrate chemistry gives insight into potential biocompatible substrates. Cell deposition and proliferation experiments were then conducted as a function of FN's surface density. Both experiments show a high FN surface density promoting cellular seeding while low protein coverage hinders cell adhesion. AFM measurements predict the protein's stiffness on more favorable substrates (hydrophilic and high FN density) is lower than on more hydrophobic surfaces or protein resistant surfaces (PEG). This provides a possible explanation as to why hydrophilic surfaces with high protein coverage have been found to be more favorable substrates for cellular seeding.[55-57]

3.2.   EXPERIMENTAL DETAILS

3.2.1.   General Procedures

All glassware was soaked at least overnight in a base bath composed of 500g of KOH (J.T. Baker (Scientific Equipment Company), Aston, PA), 500mL of tap water, and 4L of iso-Propanol (VWR International, Inc., Bridgeport, NJ). A Barnstead NANO pure filter was used to purify all water to 18MΩ·cm resistivity.   Sterile solutions and plates were used for cell experiments, and to prevent bacterial contamination, substrates for the semiaggregate experiments were placed in ethanol (Pharmco Products, Inc., Brookfield, CT) for at least an hour prior to protein and cell deposition.

3.2.2.   Solution Preparation

Phosphate buffered saline (PBS, pH = 7.2) was prepared using 10mM Na_2HPO_4 (J.T. Baker), 138mM NaCl (Sigma, St. Louis, MO), and 2.7mM KCl (Mallinckrodt, Phillipsburg, NJ). A 10µg/mL solution of fibronectin from bovine plasma (Sigma) was prepared in PBS containing 1% NaN_3 (Sigma) and stored at 4ºC. 1mM solutions for alkanethiol self-assembled monolayers (SAMs) were made by mixing the following individual compounds in ethanol (Pharmco): 1-Hexadecanethiol (Aldrich, St. Louis, MO), 11-Mercapto-1-undecanol (Aldrich), 11-Mercaptoundecanoic acid (Aldrich), and Peg(thiol)$_2$ (Molecular weight = 3400g/mol) (Shearwater Polymers, Huntsville, AL).

3.2.3.   Sample Preparation

Gold surfaces were prepared using a method developed by Hegner *et al.*[58]   Briefly, gold (99.95%) (Alfa Aesar, Ward Hill, MA) was evaporated onto freshly cleaved mica (SPI, West Chester, PA) using a Ladd Vacuum Evaporator (Ladd Research, Williston, VT).   Prior to deposition, the mica sheets were heated for several hours at 300^oC.   Surfaces were then inverted onto glass coverslips (Ted Pella, Inc., Redding, CA) using EPO-TEK 377 in a 1:1 mass ratio (Epoxy Technology, Billerica, MA), and then placed in an oven at 150^oC for ~ 1.5 hours.   Gold substrates were obtained by mechanically removing the mica with tweezers.   Remaining mica islands were negligible based on conductivity measurements.   Surfaces for SAM formation were submerged for at least 24 hours in filtered alkanethiol solution, rinsed, and briefly sonicated in ethanol prior to protein deposition.   Confirmation of SAM formation was obtained using a homemade contact angle machine ($\theta_{CH3} = 109^o$; $\theta_{OH} = 23^o$; $\theta_{COOH} = 29^o$).

For protein adsorption, a total of 25μL of 10μg/mL FN solution was exposed to each surface for 10 minutes to form a semiaggregated protein environment. For the aggregate studies, surfaces were allowed to remain in 10μg/ml FN solution at 4^oC for approximately 24 hours. All surfaces were then gently rinsed with PBS and dried using a strong flow of nitrogen before being mounted to a glass microscope slide (VMR Scientific Inc., West Chester, PA) *via* 5-minute epoxy (Devcon, Danvers, MA). Surfaces were immediately imaged in PBS at room temperature.

3.2.4. AFM Measurements/Analysis

All measurements were obtained using a molecular force probe (MFP) from Asylum Research (Santa Barbara, CA) which was capable of moving a cantilever in three dimensions for surface imaging. The instrument was controlled with Igor Pro 4.05A from Wavemetrics (Lake Oswego, OR) with all data analysis using software written in Matlab (Math Work, Inc., Natick, MA). Olympus gold-coated cantilevers with spring constants of 45 to 80 pN/nm were purchased from Asylum Research. Spring constants were determined using the thermal noise method.[59] Images were obtained in an intermittent contact mode using a tip oscillation of 60-70 nm with PBS as the imaging solvent.

For data analysis, the loading rate was obtained directly from our force plots using four data points prior to the cantilever's point of maximum extension. As discussed later, the change in the attractive force between these points combined with the sampling rate allows the loading rate experienced by the system to be determined. The velocity is then calculated using the loading rate and spring constant of the system which incorporates the spring constants of both the cantilever and the extended fibronectin chain. Bins for both force *vs*. loading rate and force *vs*. velocity plots were created to obtain approximately equal numbers of points per bin (~30 pts/bin).

3.2.5.   Cell Culture

Endothelial growth media (EGM-2MV, USA-Cambrex Bio Science Walkersville, Inc., Baltimore, MD) was thawed at $37^{o}C$ and combined with 500mL of EBM-2 basal media (USA-Cambrex Bio Science Walkersville, Inc.). Prior to combining with cells, the filtered media was placed in an incubator (Thermo Electron Corp., Model 3110, Pittsburgh, PA) for 30 minutes at $37^{o}C$. Cyropreserved Human Umbilical Vein Endothelial Cells (HUVECs) from Clonetics (USA-Cambrex Bio Science Walkersville, Inc.) were swirled in a water bath at $37^{o}C$ for 2-3 minutes and then mixed with 12mL of the HUVEC media. Cells were grown to confluence before being split.

Cell splitting was obtained by replacing the media with 5mL of Hepes's buffered saline solution (HBSS, Cambrex). Upon removal of HBSS, 5mL of a trypsin/EDTA solution (Cambrex) was added and allowed to set for 10 minutes at $37^{o}C$. Cells were then spun down at 220 gravity for 5 minutes using a Sorvall Legend RT (Kendro Laboratory, Asheville, NC) after 5mL of trypsin neutralizing solution (TNS, Cambrex) had been added. Upon removal of the supernatant, the cell pellet was re-suspended in media, and seeded onto substrates in 24 well plates (BD Bioscience) at 50,000 cells/mL per well (1mL per well). Seeded samples remained in an incubator at 5% CO_2 and $37^{o}C$ until time of analysis.

3.2.6. Hoechst Analysis

A working solution of 200µM Hoechst 33258 (Sigma) was made using sterile water. Samples remained in 1mL of solution for 10-15 minutes before placed in covered plates containing PBS or mounted directly to coverslips (Fisher Scientific, Pittsburgh, PA) using Gelvatol.

3.2.7. Fluorescent Imaging

Fluorescent images were obtained using an Olympus Provis epi-fluorescence microscope (Malvern, NY) controlled by Olympus Magnafire software and CCD camera. Images were obtained using a 10x objective, resulting in a 2.5 mm^2 image size. Cell counts were obtained using the total nuclear area and software provided by Universal Imaging Corporation (Metamorph, Version 6.1r2, Downington, PA).

3.3. THEORETICAL MODELS FOR MOLECULAR PULLING EXPERIMENTS

To investigate the mechanically induced extension of fibronectin, this study relied on two models, one used quite extensively in the literature developed from the work of Bell and Evans *et al*.[45-51] and another more recent model developed by Hummer and Szabo,[54] hereafter referred to as the Bell and Hummer models, respectively.

3.3.1. Assumptions

Both models assume the direction of the applied force, x, produces a good reaction coordinate for the system. Under applied force, this reaction coordinate is assumed to be the favored pathway in the absence of the pulling stress, therefore, giving the intrinsic thermodynamic parameters of the system. This is only valid though if all other dynamics of the system are fast compared to the one experimentally observed. Both models also assume the system's dynamics are diffusive in nature, meaning on the free energy surface, the system undergoes Brownian motion. Additional assumptions, specific to each model, are given below.

3.3.2. Bell Model

In the model developed by Bell and Evans,[45-51] an exponential relationship exists between the rate of dissociation (k_{off}) of a ligand-receptor complex and the externally applied force, F (Equation 1).

$$k_{off}(F) = k_{off}(0)e^{Fx_\beta / k_B T} \tag{1}$$

Here, $k_{off}(F)$ is the rate of dissociation under applied force, $k_{off}(0)$ is the rate of dissociation under zero applied force, x_β is the distance from the free energy minimum to the transition state projected along the direction of applied force, and $k_B T$ represents the thermal energy. Because force is applied along x, the free energy for dissociation is assumed to decrease linearly with the applied force (Equation 2).

$$\Delta G^{\ddagger}(F) = \Delta G^{\ddagger}(0) - Fx_\beta \tag{2}$$

As the mechanical force is applied to a system, the observed unbinding force will then depend on the rate at which the force is applied to the system, *i.e.* the loading rate. As Equation 3 illustrates, a logarithmic dependence of this dissociation force (F) on the loading rate (r) is predicted.

$$F = \frac{k_B T}{x_\beta} \ln\left(\frac{x_\beta r}{k_{off}^o k_B T} \right) \tag{3}$$

Over several orders of magnitude, the model expects a plot of rupture force *versus* ln(r) to reveal linear regions of increasing slope, each region corresponding to a barrier traversed along the direction of applied force. Using Equation 3 then allows x_β to be determined and extrapolating back to zero applied force, $k_{off}(0)$ and $\Delta G^\ddagger(0)$ can be determined through Equations 4 and 5, where h is Planck's constant.

$$k_{off}(0) = \frac{r \cdot x_\beta}{k_B T} \tag{4}$$

$$k_{off}(0) = \frac{k_B T}{h} e^{-\Delta G^\ddagger / k_B T} \tag{5}$$

Thus, from a loading rate plot, the thermodynamic parameters involved in ligand-receptor dissociation *via* AFM can be approximated.

However, as pointed out by Evans, application of force on proteins or highly flexible polymers results in nonlinear elastic stretches unlike a ligand-receptor scenario which displays linear elastic properties.[46-51] The model described briefly above works well for the latter case, yet complications can arise for modeling proteins and polymers. Nevertheless, Rief[60] and Carrion-Vasquez[61] have observed a linear dependence of unbinding force *versus* the logarithm of the loading rate when mechanically unfolding proteins. Therefore, this model was applied here to determine the thermodynamic parameters associated with the forced unfolding of fibronectin.

3.3.3. Hummer Model

This model assumes a molecular free energy surface ($V_o(x)$) similar to the type depicted in Figure 10 whose potential of mean force is given by Equation 6.

$$V(x,t) = V_o(x) + V_s(x - vt) \qquad (6)$$

Here, the reaction coordinate, x, is coupled to the AFM's piezo velocity, v. Hummer also assumes the free energy surface depicted in Figure 10 is characterized by Equation 7

$$BV_o(x) = \begin{cases} \dfrac{1}{2}k_m x^2 & (x < x_\beta) \\ -\infty & (x \geq x_\beta) \end{cases} \qquad (7)$$

where k_m represents the molecular spring constant, $B^{-1} = k_B T$, and x_β again corresponds to the distance from the free energy minimum to the transition state projected along the direction of applied force. Since it is assumed that the system undergoes Brownian motion on the free energy surface, Kramers theory provides the relationship between the rate of rupture in the absence of pulling ($k_{off}(0)$) and the system's properties through Equation 8.
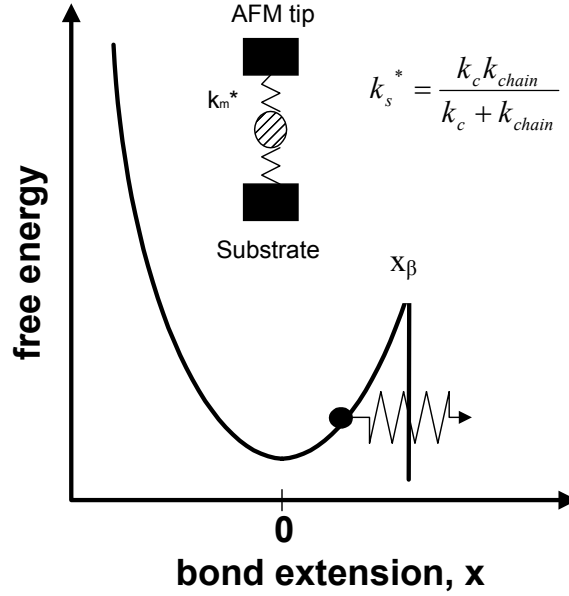
Figure 10 A free energy curve governing the rupture of the adhesive bond between an AFM tip and a chain. As the tip is pulled away from the surface, the adhesion bond is loaded by an effective spring that is created by the combination springs of the cantilever and protein. The effective spring constant, k_s^*, is obtained by fitting a line to the steeply sloped region of the force plot in Figure 12 and equating it to $k_B T k_S$. The bond spring constant, called the molecular spring constant by Hummer and Szabo,[54] is k_m^* and provides the curvature in the free energy surface seen in this figure.

$$k_{off}(0)(x_\beta; k_m) \approx (2\pi)^{-1/2} D k_m^{3/2} x_\beta e^{-B\Delta G^{\ddagger}}, \quad B\Delta G^{\ddagger} = \frac{k_m(x_\beta)^2}{2} \tag{8}$$

Here D and $\Delta G^{\ddagger}$ represent the diffusion coefficient and the unfolding barrier height, respectively.

Hummer and Szabo show how to extract the rate constant from velocity dependent pulling experiments by analyzing the statistics of the force at rupture. For intermediate pulling velocities, a fit of the average rupture force ($\overline{F}$) *versus* velocity (v) (Equation 9) allows the molecular spring constant ($k_m^* = k_B T k_m$), the barrier distance (x_β), and the kinetic offrate ($k_{off}(0)$) in the absence of pulling to be obtained.

$$BF = k_m x_\beta - \left[2k \ln \frac{k_{off}(0)e^{\gamma + k_m(x_\beta)^2/2}}{k_s v x_\beta (k_m/k)^{3/2}} \right]^{1/2} , \quad k = k_m + k_s \qquad (9)$$

Here k_s is an effective spring constant that incorporates the spring constants of both the cantilever and the extended chain, and γ is the Euler-Mascheroni constant ($\gamma = 0.5772\ldots$). Since k_s represents multiple springs in series, we can actually obtain the protein's spring constant using Equation 10 where $k_s{}^* = k_B T k_s$, and k_{chain} and k_c represent fibronectin and the cantilever's spring constant, respectively.

$$\frac{1}{k_s{}^*} = \frac{1}{k_{chain}} + \frac{1}{k_c} \qquad (10)$$

In the data reported here, the velocity was determined directly from the force plots using the loading rate and spring constant of the system as discussed earlier; therefore, a factor of $\left(1 + \dfrac{k_c k_m + k_c k_{chain}}{k_m k_{chain}} \right)$ was multiplied to v in Equation 9 to account for the tip's velocity.

3.3.4. Model Comparison

The model developed by Bell and Evans is useful for only a narrow range of rupture forces and does not allow the position of the rate-limiting barrier to fluctuate under the pulling potential, unlike the Hummer model. The Hummer model has additional advantages since the molecule's spring constant and the system's interfacial stiffness can also be determined. However, this model, with more free parameters, requires the initial inputs to be more accurate making it slightly more difficult than the Bell model in terms of ease of implementation. Furthermore, with more parameters, too much uncertainty can result if too few data points are available.

3.4.   RESULTS

3.4.1.   Mechanical Behavior of Fibronectin When Densely Populated on Surfaces

3.4.1.1.   Imaging and Molecular Pulling Measurements

Images of the prepared samples were collected in an intermittent contact mode followed by molecular pulling experiments obtained through random surface sampling.   Figure 11 shows two images collected in PBS, one of a control mica surface and one where FN was exposed to a mica substrate for approximately 24 hours.   As can be seen from the height scale and RMS roughness, FN has deposited densely on the surface.   As previously reported by us[1] and by other groups,[2-5] this higher protein density results in a more stable protein conformation and prevents domain denaturation at the surface, perhaps by protecting the domains from interacting with the substrate.[4]   In the work reported here, domain denaturation could not be studied due to poor statistics.   Focus was placed primarily on protein-protein and protein-surface interactions.
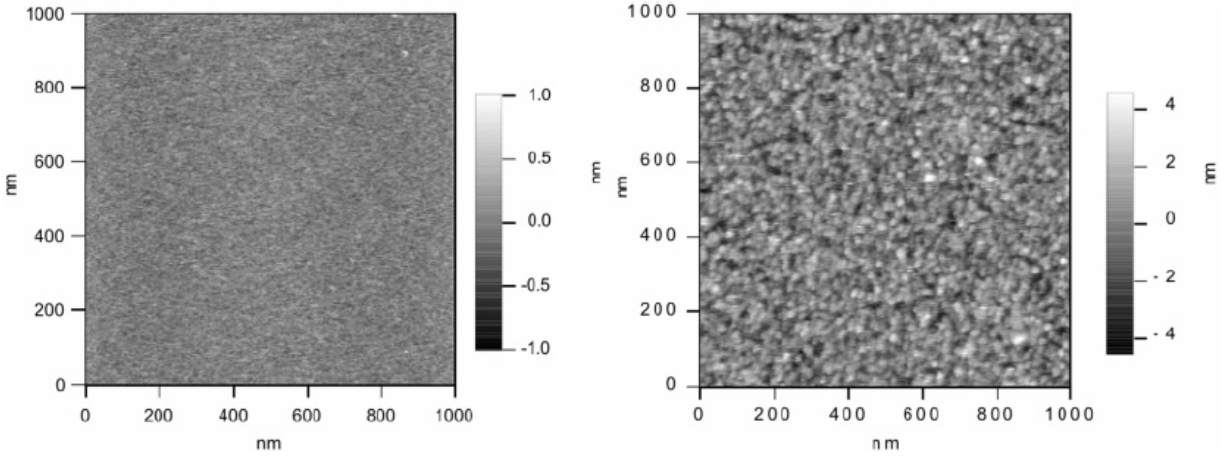
Figure 11 Height images of a control mica surface (Left, RMS roughness = 0.137 nm) and a mica substrate that was exposed to a FN solution for 24 hours at 4°C (Right, RMS roughness = 1.16 nm). The right image reflects the aggregate state of our protein studies.

A typical force plot obtained in our aggregate studies can be seen in Figure 12 while Table 4 summarizes the aggregate data collected on each substrate. The length and force for the protein ruptures were obtained using the data point at the cantilever's maximum deflection, and the difference in length (ΔL) between successive ruptures was also calculated using these points, as demonstrated by the vertical lines in Figure 12. The gray line seen on the last rupture in Figure 12 is used for gaining insight into the energy landscape the protein explores during its forced extension which will be explained in further detail shortly.
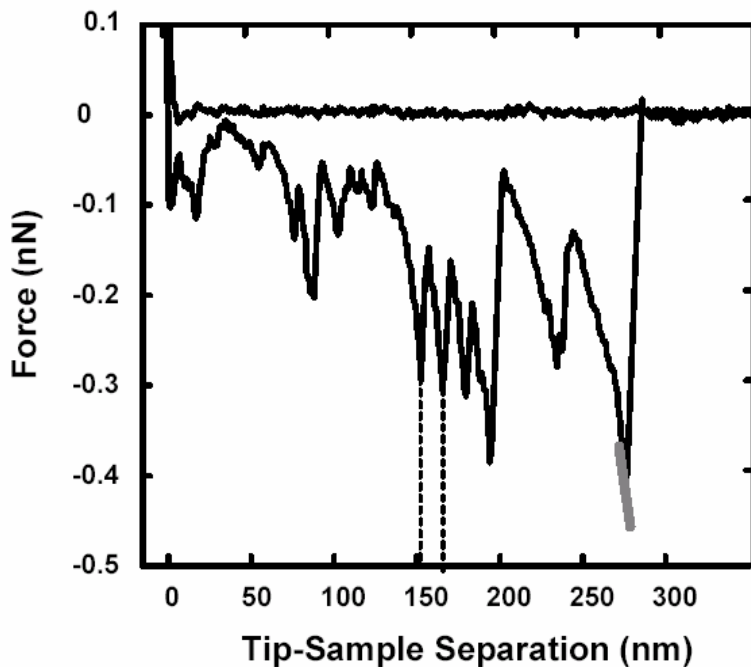
Figure 12 A typical force plot of FN densely deposited on a gold substrate. The difference in tip-sample separation between the dashed lines represent how ΔL was determined while the gray line on the last rupture illustrates the data points used to gain insight into the energy landscape the protein explores. The gray line has been extended in this figure for easier visualization.

Table 4 Summary of the Force Spectroscopy Experiments When FN is Densely Populated on Surfaces

Substrate	Total Force Plots Collected	% of Force Plots Displaying Stretching Events	Number of Ruptures Used in Analysis of Multi-Rupture Force Plots	Number of Single Rupture Force Plots
Mica	6967	15.2 %	2376	306
Gold	6952	17.7 %	2062	377
11-Mercapto-1-undecanol	7471	21.9 %	2828	542
11-Mercapto-undecanoic acid	8012	11.8 %	2059	283
1-Hexadecanethiol	9003	8.9 %	1626	280
PEG[*]	9002	0.7 %	155	23

[*]Few aggregated proteins were found on this substrate due to its resistance to protein adsorption

In Table 4, the total number of force plots obtained, the percentage of these force plots displaying force transitions after the tip-substrate rupture, and the total number of force transitions used in the data analysis are listed. Table 4 also reports the number of force plots where only one stretching event occurred after the tip-substrate rupture. These elastic responses, as will be shown below, are important for probing a specific protein-tip interaction, giving insight into how a substrate affects the binding regions accessible for AFM tip attachment. From Table 4, the lowest extension probabilities were found on PEG (which is known to inhibit protein

adsorption) and the $-CH_3$ terminating SAM. The highest extension probabilities occur for the most part on the more hydrophilic surfaces: mica, a hydroxyl-terminated SAM (-OH), and a bare gold substrate. We were slightly surprised at the higher extension percentage obtained on gold since the protein's exposed sulfhydryl groups could form multiple covalent attachments to the substrate, preventing protein elongation. The SAM functionalized with a terminating carboxylic acid group (-COOH) displayed protein extension probabilities in between the more hydrophobic and hydrophilic surfaces.

3.4.1.2.   Modeling the Aggregate Data

To model the protein extension data using the theories described previously, the loading rate was calculated using the data point at the cantilever's maximum extension and four points prior to this rupture point, seen as a gray line in Figure 12. We emphasize that the gray line seen in Figure 12 is used only to show the location of the data points used for each rupture. Equation 11 illustrates how the loading rate was determined from our AFM force plots.

$$r_{rupture} = \frac{\Delta F \cdot S_{rate}}{n+1} \tag{11}$$

Here, ΔF is the change in the attractive force from the point of rupture to four points prior to this rupture, n is 1 less than the number of points used to obtain ΔF, and S_{rate} is the sampling rate in the data acquisition in points/s. Velocity for fits to the Hummer model were then obtained from the loading rate and spring constant of the system.

Figure 13 shows data fit to both the Bell and Hummer models while Tables 5 and 6 summarize the corresponding parameters obtained using the mean values for force, loading rate, and velocity. The parameters in Table 5 were determined from force plots containing multiple

elastic responses but excludes the last rupture which is indicative of final protein-tip detachment. Table 6 probes a specific protein-tip interaction since these parameters arise from force plots containing a single elastic response. Comparison of the parameters obtained from both models can be difficult since the Bell model often predicts multiple barriers being traversed in the direction of applied force while the Hummer model often indicates a single barrier for the same data set. In Table 6, where both models predict only a single barrier, the *trend* for x_β, $\Delta G^\ddagger$, and $k_{off}(0)$ are identical for both models, but interestingly, the *values* obtained can vary quite dramatically between the two models. As Hummer states, this results from the narrow range over which the Bell expression is valid. We note that the assumption by Bell of an activation prefactor of $k_B T/h$ is also significant. In general though, for both data sets represented in Tables 5 and 6, the Hummer model tends to predict higher values for the barrier position (x_β) and lower values for the barrier heights ($\Delta G^\ddagger$). Both models predict a very stiff protein conformation on PEG as evident by the short barrier position and further confirmed by the large k_s and $k_m{}^*$ values from the Hummer model. Elaboration on this key point and PEG's inertness is examined in more detail later.
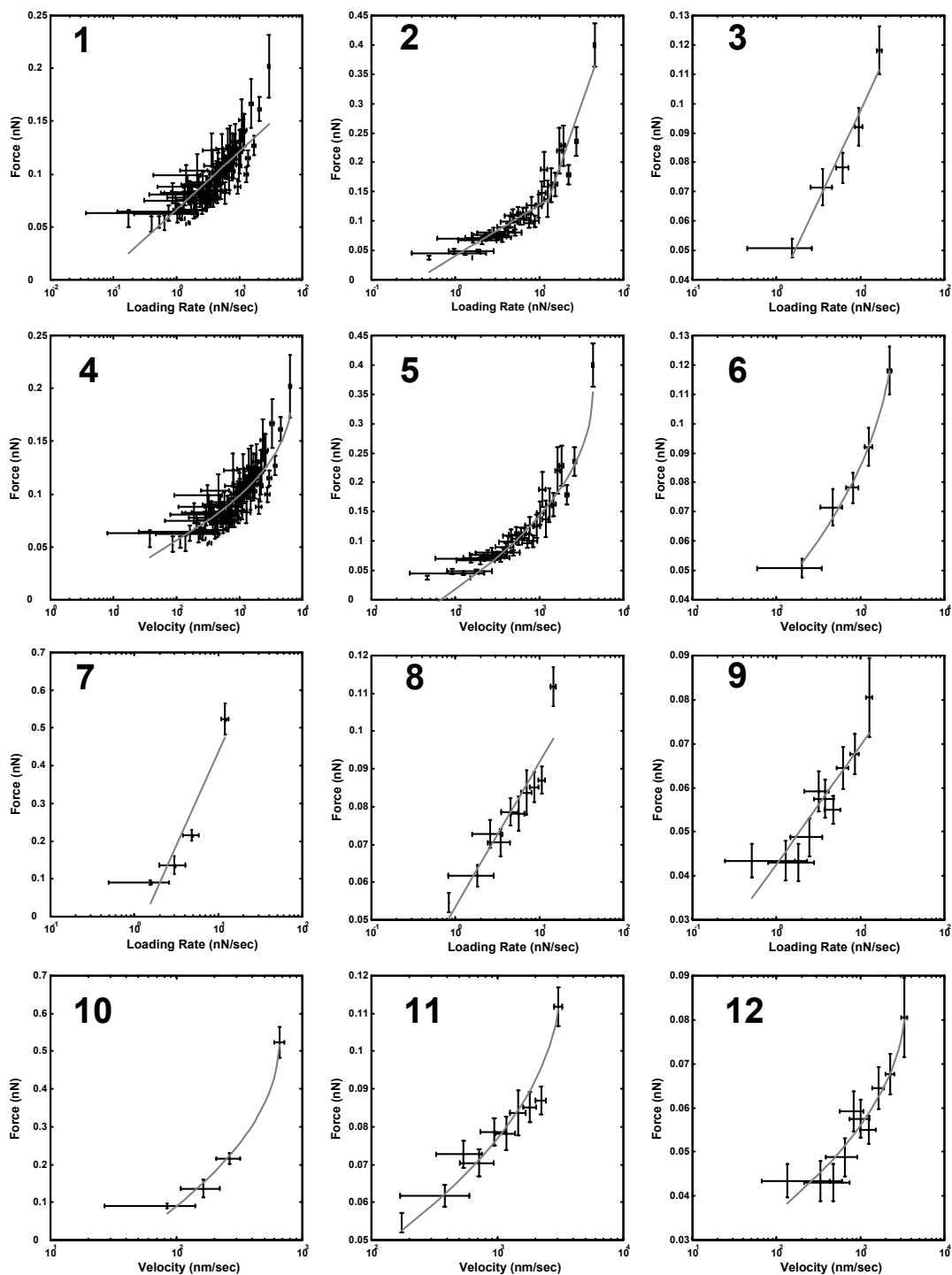
Figure 13 Plots of data fit by both the Bell (Force *vs.* Loading Rate; Rows 1 and 3) and Hummer models (Force *vs.* Velocity; Rows 2 and 4). 1 & 4: Mica/aggregated/multirupture; 2 & 5: -OH terminated SAM/semiaggregated/multirupture; 3 & 6: -CH$_3$ terminated SAM/aggregated/single rupture; 7 & 10: PEG/aggregated/multirupture; 8 & 11: -OH terminated SAM/aggregated/single rupture; 9 & 12; mica/aggregated/single rupture. Parameters from these fits can be found in Tables 5, 6, 9, and 10.

53

Table 5 Thermodynamic Parameters for the Forced Extension of Aggregated Fibronectin Using Multi-Ruptured Force Plots

Substrate	Bell/Evans Model			Hummer Model[#]					
	x_β (nm)	$k_{off}(0)$ (s^{-1})	$\Delta G^{\ddagger}(0)$ (kcal/mol)	k_s (nm^{-2})	$k_m{}^*$ (N/m)	x_β (nm)	$k_{off}(0)$ (s^{-1})	$\Delta G^{\ddagger}(0)$ (kcal/mol)	D (nm^2/s)
Mica	0.17 ± 0.01	3 ± 0.7	16.7 ± 0.2	1.1	0.52	0.36	5	4.9	102
11-Mercapto- 1-undecanol	0.18 ± 0.01 6E-3 ± 3E-4	1 ± 0.4 18 ± 4	17.0 ± 0.2 15.5 ± 0.1	1.5	0.66	0.36	2	6.0	151
11-Mercapto- undecanoic acid	0.12 ± 8E-3 7E-3 ± 8E-4	4 ± 0.8 25 ± 14	16.4 ± 0.1 15.4 ± 0.3	2.5	5.6	0.13	17	7.1	1185
1-Hexadecanethiol	0.11 ± 0.01 3E-3 ± 4E-4	4 ± 0.7 14 ± 9	16.5 ± 0.1 15.7 ± 0.4	2.5	5.6	0.12	17	5.6	106
Gold	0.10 ± 0.01 0.01 ± 1E-3	11 ± 2 42 ± 20	15.9 ± 0.1 15.0 ± 0.3	3.4	3.2	0.11	38	2.6	3
PEG	0.02 ± 4E-3	6 ± 3	16.2 ± 0.3	4.5	13	0.04	18	1.6	0.1

[#]Values typically showed less than 2% deviation.

Table 6 Parameters for the Forced Extension of Aggregated Fibronectin Using Force Plots Containing A Single Rupture

Substrate	Bell/Evans Model			Hummer Model[#]					
	x_β (nm)	$k_{off}(0)$ (s^{-1})	$\Delta G^{\ddagger}(0)$ (kcal/mol)	k_s (nm^{-2})	$k_m{}^*$ (N/m)	x_β (nm)	$k_{off}(0)$ (s^{-1})	$\Delta G^{\ddagger}(0)$ (kcal/mol)	D (nm^2/s)
Mica	0.35 ± 0.06	2 ± 1	16.8 ± 0.4	0.94	0.08	1.1	0.4	6.7	917
11-Mercapto-1-undecanol	0.24 ± 0.03	2 ± 1	16.7 ± 0.3	1.2	0.18	0.66	1	5.6	261
11-Mercapto-undecanoic acid	0.16 ± 0.04	9 ± 6	15.9 ± 0.4	1.8	0.31	0.44	9	4.3	121
1-Hexadecanethiol	0.15 ± 0.02	10 ± 3	15.9 ± 0.2	1.9	0.33	0.41	12	4.0	91
Gold	0.13 ± 0.02	17 ± 6	15.6 ± 0.2	2.5	0.44	0.33	20	3.4	48

[#]Values typically showed less than 2% deviation.

Table 7 contains the results of FN's spring constant after correcting the effective force constant to account for the cantilever's spring constant (Equation 10). As can be seen in this table, fibronectin's rigidity is statistically *dependent* upon the substrate's composition and as we will show later, FN's surface density. Additionally, the diffusion coefficient for motion along the rupture reaction coordinate can be obtained from Hummer's model and is provided in Tables 5 and 6.

Table 7 Fibronectin's Rigidity (k_{chain}) When Aggregated On A Substrate

Substrate	Force Plot Type	$k_{chain,}$ (nN/nm)[*]
Mica	Multi-rupture	5.0E-3 ± 7.2E-5
	Single rupture	4.0E-3 ± 1.7E-4
11-Mercapto-1-undecanol	Multi-rupture	6.8E-3 ± 1.7E-4
	Single rupture	5.2E-3 ± 1.5E-4
11-Mercaptoundecanoic acid	Multi-rupture	1.2E-2 ± 2.5E-4
	Single rupture	8.0E-3 ± 2.8E-4
1-Hexadecanethiol	Multi-rupture	1.2E-2 ± 3.6E-4
	Single rupture	8.4E-3 ± 3.2E-4
Gold	Multi-rupture	1.8E-2 ± 3.8E-4
	Single rupture	1.2E-2 ± 5.7E-4
PEG	Multi-rupture	2.5E-2 ± 2.8E-3
	Single rupture	Poor statistics

[*]These values assumed a 10% error in the determination of the cantilever's spring constant.

3.4.2.   Mechanical Behavior of Fibronectin When Semiaggregated on Surfaces

3.4.2.1.   Imaging and Molecular Pulling Measurements

Figure 14 shows an image collected when fibronectin was exposed to a mica surface for 10 minutes and again imaged in PBS using an intermittent contact mode. As can be seen in this image, the proteins are not isolated as in the case of our single molecule studies reported earlier[1] nor are they in a saturated environment as seen in Figure 11. Throughout this paper, this state of protein deposition will be referred to as a semiaggregate form.
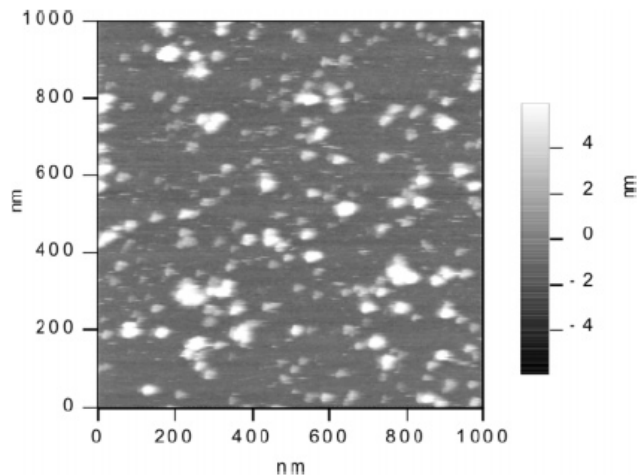
Figure 14 Height image of a mica substrate that was exposed to a 10 μg/ml solution of FN for 10 minutes (RMS roughness = 1.85 nm). This state is referred to as our semiaggregate form where the proteins are neither completely isolated nor completely aggregated.

Table 8 summarizes the type of force plots observed for surfaces with this lower protein deposition. Elongation on a gold substrate resulted in the fewest occurrences of protein extension which although not seen in the aggregated samples might reflect more covalent attachments with the substrate. Similar extension probabilities for SAMs terminated in a –OH and –CH$_3$ group were obtained followed by a –COOH terminated SAM and mica. Because of poor statistics, we do not have any information of FN in a semiaggregate form on PEG. Closer examination of Table 8 reveals a similarity with the aggregate work; the percentage of ruptured force plots displaying a single elastic response reflect a correlation with the substrate's chemistry. In this case, a –OH terminated surface (32%) and mica (40%) display the fewest single rupture force plots, followed by a gold substrate (50%), –COOH terminated surface (52%), and finally the more hydrophobic SAM, -CH$_3$ (63%). Therefore, it is more probable to see multiple elastic responses on hydrophilic surfaces.

Table 8 Summary of the Force Spectroscopy Experiments When FN is Semiaggregated on Surfaces

Substrate	Total Force Plots Collected	% of Force Plots Displaying Stretching Events	Number of Ruptures Used in Analysis of Multi-Rupture Force Plots	Number of Single Rupture Force Plots
Mica	11918	8.4 %	1314	401
Gold	10029	2.0 %	292	97
11-Mercapto-1-undecanol	10211	6.0 %	1158	198
11-Mercapto-undecanoic acid	13085	7.1 %	994	479
1-Hexadecanethiol	7995	6.0 %	465	303

3.4.2.2.   Modeling the Semiaggregate Data

Tables 9 and 10 give the corresponding thermodynamic and kinetic parameters obtained from using the Bell and Hummer models while Table 11 shows FN's rigidity when semiaggregated on a surface. When compared to Table 7, the protein adopts a more rigid conformation in the semiaggregate state as a result of more substrate-protein interactions.

Table 9 Thermodynamic Parameters for the Forced Extension of Semiaggregated Fibronectin Using Multi-Ruptured Force Plots

Substrate	Bell/Evans Model			Hummer Model[#]					
	x_β (nm)	$k_{off}(0)$ (s^{-1})	$\Delta G^{\ddagger}(0)$ (kcal/mol)	k_s (nm^{-2})	k_m^* (N/m)	x_β (nm)	$k_{off}(0)$ (s^{-1})	$\Delta G^{\ddagger}(0)$ (kcal/mol)	D (nm^2/s)
Mica	0.27 ± 0.03	5 ± 2	16.3 ± 0.2	1.7	0.44	0.35	22	3.8	94
	$0.02 \pm 4E\text{-}3$	54 ± 44	15.0 ± 0.5						
11-Mercapto-1-undecanol	0.11 ± 0.01	9 ± 2	16.0 ± 0.1	2.6	3.7	0.10	52	2.4	3
	$0.02 \pm 4E\text{-}3$	33 ± 22	15.2 ± 0.4						
11-Mercapto-undecanoic acid	0.10 ± 0.01	9 ± 3	15.9 ± 0.2	5.2	8.5	0.06	32	2.3	0.7
	$0.01 \pm 2E\text{-}3$	34 ± 27	15.1 ± 0.5						
1-Hexadecanethiol	0.08 ± 0.02	7 ± 4	16.1 ± 0.3	2.6	2.0	0.16	15	3.4	8
Gold	0.04 ± 0.01	10 ± 5	16.0 ± 0.3	5.2	6.1	0.08	8	2.9	0.6

[#]Values typically showed less than 2% deviation.

Table 10 Thermodynamic Parameters for the Forced Extension of Semiaggregated Fibronectin Using Force Plots Containing A Single Rupture

Substrate	Bell/Evans Model			Hummer Model[#]					
	x_β (nm)	$k_{off}(0)$ (s^{-1})	$\Delta G^\ddagger(0)$ (kcal/mol)	k_s (nm^{-2})	k_m^* (N/m)	x_β (nm)	$k_{off}(0)$ (s^{-1})	$\Delta G^\ddagger(0)$ (kcal/mol)	D (nm^2/s)
Mica	1.38 ± 0.45 0.09 ± 0.01	0.01 ± 0.04 49 ± 20	19.9 ± 2.0 15.0 ± 0.2	1.4	0.41	0.29	135	2.5	81
11-Mercapto-1-undecanol	0.09 ± 0.03	24 ± 20	15.5 ± 0.5	2.7	0.94	0.18	66	2.3	13
11-Mercapto-undecanoic acid	0.14 ± 0.01 $0.02 \pm 3E\text{-}3$	13 ± 3 51 ± 43	15.7 ± 0.1 14.9 ± 0.5	5.3	3.1	0.10	46	2.3	3
1-Hexa-decanethiol	0.11 ± 0.01	22 ± 7	15.4 ± 0.2	2.6	1.5	0.17	62	3.1	27
Gold	0.08 ± 0.02	11 ± 10	15.9 ± 0.6	5.4	0.87	0.28	0.81	4.8	9

[#]Values typically showed less than 2% deviation.

Table 11 Fibronectin's Rigidity (k_{chain}) When Semiaggregated On a Substrate

Substrate	Force Plot Type	$k_{chain,}$ (nN/nm)[*]
Mica	Multi-rupture	7.9E-3 ± 5.7E-4
	Single rupture	6.2E-3 ± 4.7E-4
11-Mercapto-1-undecanol	Multi-rupture	1.3E-2 ± 5.0E-4
	Single rupture	1.4E-2 ± 1.2E-3
11-Mercaptoundecanoic acid	Multi-rupture	3.1E-2 ± 1.2E-3
	Single rupture	3.1E-2 ± 1.9E-3
1-Hexadecanethiol	Multi-rupture	1.2E-2 ± 4.9E-4
	Single rupture	1.2E-2 ± 4.4E-4
Gold	Multi-rupture	3.9E-2 ± 1.4E-3
	Single rupture	4.2E-2 ± 1.8E-3

[*]These values assumed a 10% error in the determination of the cantilever's spring constant.

3.5.   DISCUSSION

3.5.1.   Surface Chemistry's Affect on Fibronectin

3.5.1.1.   Aggregate Data

Examination of the k_{chain} values in Table 7 (mica < -OH < -COOH < -CH$_3$ < Au < PEG) shows FN adopting a less rigid conformation on more hydrophilic surfaces. The more hydrophobic or unfavorable the surface, the more rigid FN becomes. When adsorbed on a gold and PEG coated surface, FN displays the highest rigidity which for gold could result from the presence of covalent bonds between gold and FN's sulfhydryl and disulfide groups. Zhou *et al.*[62]

have shown this particular type of chemistry occurring in their electrochemical studies of cytochrome c on gold electrodes. An explanation of FN's rigidity on PEG and PEG's inertness will be addressed shortly.

The ability to elongate FN with an AFM probe is related to the protein's rigidity. Table 7 generally shows a decrease in protein extension probability (PEG < -CH$_3$ < -COOH < mica < Au < -OH) as the surface hydrophobicity increases. As stated earlier, we were surprised at the higher extension probability obtained on gold, but the remaining surfaces indicate a decrease in FN extension probability when adsorbed on more hydrophobic substrates. As Cheng et al.[29] and Culp et al.[30] state, FN undergoes greater denaturation of its secondary structure on hydrophobic surfaces. Subsequently, an increase in substrate binding affinity is also observed for more hydrophobic surfaces.[27-28] Because of the greater denaturation of FN's domains and the stronger binding affinity on hydrophobic surfaces, we would expect lower extension probabilities (likelihood to bind to the AFM tip) and higher protein rigidities. This agrees with the trends we have observed for FN extension via AFM, but we have provided the first quantitative measure of FN's rigidity on these surfaces.

Table 6 which addresses FN's detachment from a gold-coated AFM probe reveals a surface's influence on the exposed protein regions accessible to the AFM tip. For these single rupture force plots, we find both models predict longer barrier positions (x_β) (Au < -CH$_3$ < -COOH < -OH < mica), higher barrier heights ($\Delta G^{\ddagger}$) (Au < -CH$_3$ < -COOH < -OH < mica), and slower kinetic offrates ($k_{off}(0)$) (mica < -OH << -COOH < -CH$_3$ < Au) for more hydrophilic surfaces. As stated above, we found that FN adopted a looser, more flexible conformation on hydrophilic surfaces (Table 7 and k_s in Table 6) resulting in higher extension probabilities. Because these conformations are more flexible, the ability to distort the molecule before a

transition occurs is greater, producing more distant barrier positions. As Figure 10 illustrates, the longer the barrier distance, the higher the barrier height and slower the kinetic offrate become, a result obtained here for the single rupture force plots.

The diffusion rate constants for the single rupture force plots also show a systematic trend. Faster diffusion coefficients are found for proteins adsorbed to hydrophilic substrates. This is consistent with the looser conformations shown earlier (implied by the lower chain spring constants) and will be compared with results from other measurements, below.

Examining force plots containing multiple elastic responses (Table 5: Hummer Model), we found more hydrophilic surfaces producing more distant barrier positions (PEG < Au < -CH$_3$ < -COOH < -OH, mica) and slower offrates (-OH < mica << -COOH, -CH$_3$ < PEG << Au). The barrier heights though did show variations which cannot be explained at this time. Interestingly, the barrier position for FN adsorbed on PEG displayed the shortest distance of all but an apparently unphysical distance. A more familiar barrier position might be obtained if it is assumed that the direction of applied force is at a considerable angle to the initial direction for surface dissociation, but the validity of this assumption[63-69] is beyond the scope of this work. Similar parameter trends are also obtained with the Bell model when using the barrier traversed more frequently as evident by the data's point density.

3.5.1.2. Semiaggregate Data

Results from the semiaggregate studies did not show obvious correlations based on substrate chemistry. For instance, the order of k$_{chain}$ (Table 11) for both single and multiple rupture force plots is mica < -CH$_3$ < -OH < -COOH < Au. Similar sequences which lack substrate chemistry dependence can be found for the additional parameters listed in Tables 9 and

10. Because the semiaggregate state provides insight into the early stages of nonspecific protein adsorption, the inconsistent trends suggest multiple, irreversibly bound protein conformations exist on each substrate.

3.5.1.3. Comparison of Aggregate and Semiaggregate Data

When comparing *corresponding substrates* with *corresponding force plot types* (single *vs*. multi-rupture), the semiaggregate and aggregate studies reveal several trends. The effective spring constant (k_s) and the interfacial rigidity (k_m^*) in Tables 5, 6, 9, and 10 show the protein adopting a stiffer conformation in the semiaggregate studies. Tables 7 and 11 show similar results for FN's rigidity when correcting for the cantilever's spring constant. This likely results from the protein's increased surface exposure since few neighboring proteins cannot prevent a FN molecule from undergoing surface denaturation. Because of the stiffer conformations in the semiaggregate studies, shorter x_β values and for the most part, lower barrier heights and higher kinetic offrates were obtained as predicted by Figure 10. In addition, comparison of k_m^* for the single rupture force plots (Tables 6 and 10) on corresponding surface types shows the interfacial stiffness is affected by the presence of neighboring proteins. Extension of proteins in a semiaggregate state show higher interfacial rigidities than when the proteins are aggregated, suggesting additional surface binding. Excluding mica and a $-CH_3$ terminating SAM, this trend is also observed for the multi-ruptured force plots.

3.5.2.   Correlations Between the Hummer Model's Fit Parameters

In the work reported here, some of the Hummer parameters were found to correlate linearly with the force and extension of FN. Figure 15 shows the correlations between the peak length to an elastic response, k_{chain}, k_m^*, and the rupture force. As can be seen in this Figure, when fibronectin's rigidity increases (k_{chain}), the length to which we can extend the protein decreases linearly while the rupture force for these extensions increases. Similarly, as the interfacial stiffness of FN increases, the ability to elongate the protein from the substrate decreases linearly as well. In the plot of ΔL *vs*. k_{chain}, PEG was omitted from the fit because of its deviation from the trend.
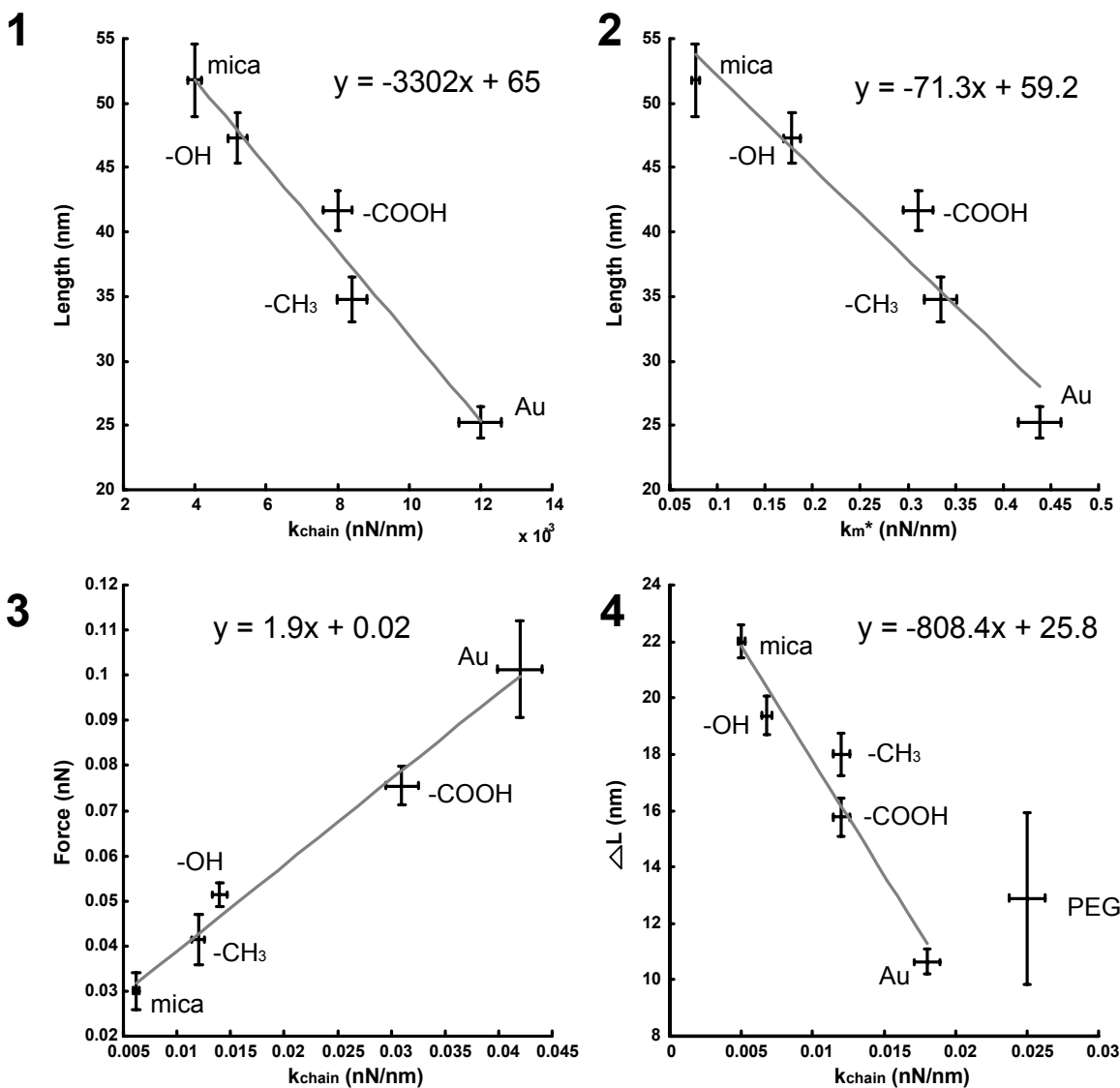
Figure 15 Correlations obtained in the aggregate (1, 2, 4) and semiaggregate (3) experiments for force plots containing a single (1-3) or multiple (4) elastic response. As FN's rigidity (k_{chain}) or interfacial stiffness (k_m^*) increases, the length to which the chain can be extended *via* AFM decreases. For these plots, peak lengths and rupture forces were obtained by a Lorentzian or Gaussian fit to the data. For the last figure, one data point, representing PEG, was omitted from the fit.

3.5.3.   Multiple Barrier Events

In the higher velocity regime of our AFM experiments, three data sets displayed a possible multiple barrier process being overcome in FN's forced extension. Figure 16 shows these force *versus* velocity plots fit to the Hummer model. As can be seen in this Figure, another region where the rupture force is increasing rapidly as a function of velocity exists. This could result in a change of velocity dependence where now stochastic motions would no longer dominate the unbinding dynamics, resulting in a $v^{1/2}$ dependence rather than a logarithmic dependence on velocity.[54]   However, in this limit of fast pulling, Hummer states the piezo velocity, v, must greatly exceed $(k_{off}(0)(x_\beta k_s)^{-1}\exp(k_m(x_\beta)^2/2)$.[54] Using the parameters from Table 5 and our velocity, stochastic fluctuations have not become irrelevant at these velocities; therefore, it is plausible this region corresponds to another barrier.   The thermodynamics for this process, however, cannot be estimated at this time because less than 5% of the data occurs in this region. Furthermore, because of the small percentage of data points, the parameter values listed in Table 5 are not significantly affected from the second possible barrier.
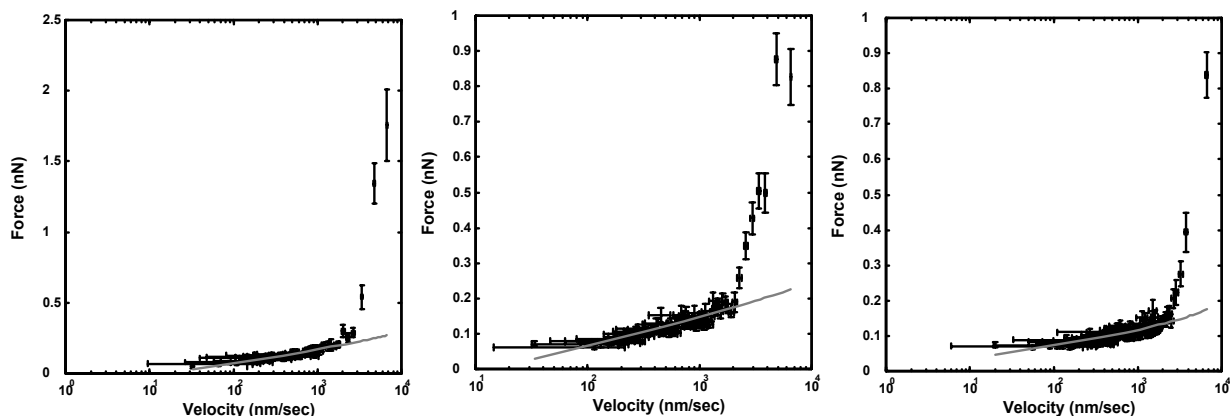
Figure 16 Force *vs*. velocity plots of FN adsorbed on a -CH$_3$ (left), -COOH (middle), and -OH (right) terminating SAM.   All graphs were fit to the Hummer model[54] and represent data obtained in the aggregate studies with force plots displaying multiple elastic responses. The last rupture, indicative of final protein-tip detachment, was excluded from these plots. The rapid increase in rupture force at higher velocities suggests an additional barrier overcome in FN's forced extension and is not an indication of a region where stochastic motion has become irrelevant.

3.5.4.   Why might PEG inhibit protein adsorption?

Since the early 1980s, PEG has been used quite extensively for preventing or minimizing nonspecific protein adsorption on surfaces, in particular, surfaces for biomedical applications. PEG's ability to inhibit a proteineaceous film's growth has been explained primarily by a theory based on excluded volume effects and steric stabilization.[70-73]   It is believed that the high conformational freedom of the PEG chains near the surface contributes to the surface's inertness. Higher PEG concentrations with longer chain lengths have been found to provide increased protein resistance[74-75] although this resistance does reach a limit as a function of chain length.

A low extension probability for FN on PEG was observed (0.7% of collected force plots) which is consistent with previous experiences.[70-75]   The proteins that do bind to PEG though

exhibit interesting properties. As can be seen in Table 5, FN's interfacial stiffness on a PEG surface ($k_m{}^* = 13$ N/m) is much higher than on the other surfaces examined here (0.5-5.6 N/m). The rigidity of FN chains (k_{chain}) is also highest on this substrate (Table 7). We conclude therefore that FN exists in a volume restricted state when on or within PEG. Hence, entropic costs to adsorption are paid by both the protein and PEG chains. The fitted parameters from the Hummer model also indicate the protein is destabilized in this environment ($\Delta G^{\ddagger} = 1.6$ kcal/mol).

3.5.5. AFM's Correlation With Cell Deposition Experiments

HUVEC cells were deposited on two surfaces for each substrate type and examined on day 7. Figure 17 shows two fluorescence images of cells deposited on –CH$_3$ terminated SAMs with FN in a semiaggregate and aggregate form while Table 12 gives the averaged cell count results. Cell counts were obtained by averaging 8 images, 4 images per surface with 2 surfaces per substrate type. Due to surface rinsing and different cell binding affinities on the various surface types, we do not attempt any correlations between *different* surface types. However, we can compare the overall averages of cell adsorption on control (804), semiaggregate (719), and aggregate surfaces (944). It appears that a semiaggregate form of FN inhibits cell deposition. In addition, when comparing similar surface types, *i.e.* a gold surface with semiaggregated FN and a gold control, except for the –OH terminating SAM, all cell counts for the semiaggregate samples display lower averages. It is worth noting that the two substrates for the –OH surface displayed significantly different cell counts, so it is possible that this value could still exceed the semiaggregate protein cell count.
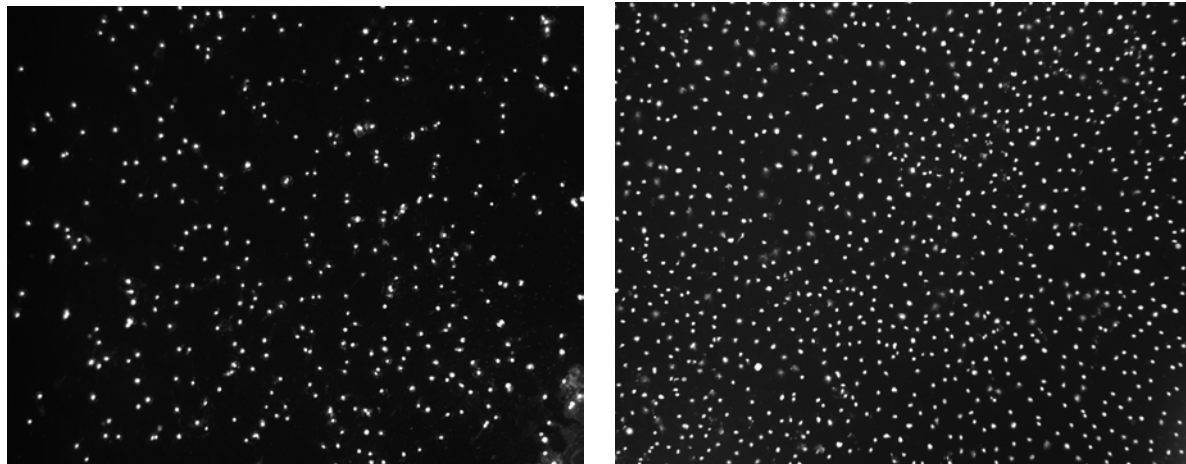
Figure 17 Fluorescent images (nuclear staining; image size = 2.5 mm^2) of HUVEC cells deposited on –CH$_3$ terminated SAMs with FN in a semiaggregate (Left; Cell count = 365) and aggregate form (Right; Cell Count = 993). FN in an aggregate form promoted cell deposition and proliferation while FN in a semiaggregate state inhibited cell proliferation (See Table 12).

We find that FN in an aggregate state promotes additional cellular seeding. Comparison of *similar* surface types in Table 12 show higher individual cell averages for FN in an aggregate state than in a semiaggregate state. This strongly correlates with the AFM work presented here. In the force-extension experiments, domain unfolding events were *only* observed in the aggregate protein studies reflecting the surface denaturation of FN in a semiaggregate environment prior to its extension. This concept of FN's surface density influencing its stability provides one explanation as to why one should expect the cell counts to be lower on our semiaggregate protein surfaces. Further examination of the parameters obtained from the Hummer model also suggests increased difficulty for a cell to reorganize the underlying proteins when in a semiaggregate environment. As stated earlier, all k$_s$ and the majority of the k$_m$* values were higher for the semiaggregate experiments. Above, we suggested the stiffer protein might

be due to increased protein-substrate binding as further supported by the greater frequency of single rupture force plots, both indicating the ability to extend FN was limited. Perhaps proteins adopting stiffer conformations hinder a cell's ability to reorganize the adsorbed FN, making these substrates less favorable for cell deposition. These results indicate there might be a correlation between AFM and cell deposition experiments which could provide information valuable for biocompatibility studies, although additional testing is required.

Table 12 HUVEC Cell Counts For Aggregated and Semiaggregated Substrates After 7 Days of Being Seeded

Substrate	Cell Count for Control Surfaces*	Cell Count for Semiaggregated Surfaces	Cell Count for Aggregated Surfaces
Gold	900 ± 17	716 ± 55	880 ± 17
Mica	908 ± 28	828 ± 22	940 ± 21
11-Mercapto-1-undecanol	289 ± 61	486 ± 25	851 ± 14
11-Mercaptoundecanoic acid	998 ± 10	826 ± 14	959 ± 8
1-Hexadecanethiol	925 ± 12	738 ± 48	1088 ± 13
Average	**804** ± 26	**719** ± 33	**944** ± 15

*Control surfaces reflect the amount of nonspecific adsorption when FN is absent from the substrate.

3.6. CONCLUSIONS

The mechanical behavior of FN molecules that are elongated between an AFM tip and a variety of substrates was measured, modeled, and compared to cell seeding experiments. Proteins were examined at two surface concentrations, one with a high surface density of protein with multiple intermolecular interactions referred to as the aggregate state and another state where the proteins were not completely isolated but were also not densely deposited. This condition was referred to as the semiaggregate state.

Modeling of the force-extension data using two different theories resulted in similar trends for the fitted thermodynamic parameters from which insight into the protein's binding state could be obtained. Aggregated proteins adsorbed on hydrophobic surfaces adopted more rigid conformations while looser conformations were observed on more hydrophilic surfaces. Studies of FN in a semiaggregate state showed heterogeneity in the model's thermodynamic parameters suggesting that in the early stages of nonspecific adsorption, multiple protein conformations exist, each having bound irreversibly to the substrate. Additionally, the magnitudes of the diffusion coefficients we obtained are roughly similar to those found by Wertz and Santore[76] in protein spreading experiments on albumin and fibrinogen. Finally, the force spectroscopy experiments were compared to cellular seeding experiments. As predicted from the models used in this work, surfaces with aggregated FN promoted cellular deposition while surfaces with FN in a semiaggregate state appeared to hinder cellular deposition and growth. AFM's correlation with cell experiments looks promising although additional testing is required.

BIBLIOGRAPHY

1. Meadows, P. Y.; Bemis, J. E.; Walker, G. W. *Langmuir,* **2003**, 19, 9566.

2. Norde, W.; Favier, J. P. *Colloids Surfaces*. **1992**, 64, 87.

3. Brash, J. L.; Horbett, T. A., Eds. *Proteins at Interfaces II: Fundamentals and Applications*. American Chemical Society: Washington, DC, 1995.

4. Grinnell, F.; Feld, M. K. *J. Biomed. Mater. Res*. **1981**, 15, 363.

5. Steadman, B. L.; Thompson, K. C.; Middaugh, C. R.; Matsuno, K.; Vrona, S.; Lawson, E. Q.; Lewis, R. V. *Biotechnol. Bioeng*. **1992**, 40, 8.

6. Lestelius, M.; Liedberg, B.; Tengvall, P. *Langmuir*. **1997**, 13, 5900.

7. Scotchford, C. A.; Gilmore, C. P.; Cooper, E.; Leggett, G. J.; Downes, S. *J. Biomed. Mater. Res*. **2002**, 59, 84.

8. Sigal, G. B.; Mrksich, M.; Whitesides, G. M. *J. Am. Chem. Soc*. **1998**, 120, 3464.

9. Mrksich, M. *Cell. Mol. Life Sci*. **1998**, 54, 653.

10. Kidoaki, S.; Matsuda, T. *Langmuir*. **1999**, 15, 7639.

11. Denis, F. A.; Hanarp, P.; Sutherland, D. S.; Gold, J.; Mustin, C.; Rouxhet, P. G.; Dufrene, Y. F. *Langmuir*. **2002**, 18, 819.

12. McFarland, C. D.; Thomas, C. H.; DeFilippis, C.; Steele, J. G.; Healy, K. E. *J. Biomed. Mater. Res*. **2000**, 49, 200.

13. Dufrene, Y. F.; Marchal, T. G.; Rouxhet, P. G. *Langmuir*. **1999**, 15, 2871.

14. Tripp, B. C.; Magda, J. J.; Andrade, J. D. *J. Colloid Interface Sci*. **1995**, 173, 16.

15. Tegoulia, V. A.; Cooper, S. L. *J. Biomed. Mater. Res*. **2000**, 50, 291.

16. Prime, K. L.; Whitesides, G. M. *Science,* **1991**, 252, 1164.

17. Tidwell, C. D.; Ertel, S. I.; Ratner, B. D. *Langmuir,* **1997**, 13, 3404.

18. Franco, M.; Nealey, P. F.; Campbell, S.; Teixeira, A. I.; Murphy, C. J. *J. Biomed. Mater. Res*. **2000**, 52, 261.

19.   Muir, D.; Manthrope, M.   *J. Cell Biol.* **1992**, 116, 177.

20.   Miyamoto, S.; Katz, B. Z.; Lafrenie, R. M.; Yamada, K. M.   *Ann. N.Y. Acad. Sci.* **1998**, 857, 119.

21.   Clark, R. A. F.   *Dermat. Clin.* **1993**, 11, 647.

22.   McDonagh, J.; Ed. *Plasma Fibronectin, Structure and Function*; Marcel Dekkar: New York, 1985.

23.   Mosher, D.; Ed. *Biology of Extracellular Matrix: A Series Fibronectin*; Academic Press: San Diego, 1989.

24.   Baugh, L.; Vogel, V. *J. Biomed. Mater. Res.*, **2004**, 69, 525.

25.   Price, T. M.; Rudee, M. L.; Pierschbacher, M.; Ruoslahti, E.   *Eur. J. Biochem*, **1982**, 129, 359.

26.   Bergkvist, M.; Carlsson, J.; Oscarsson, S. *J. Biomed. Mater. Res.*, **2003**, 64A, 349.

27.   Pettit, D. K.; Horbett, T. A.; Hoffman, A. S. *J. Biomed. Mater. Res.*, **1992**, 26, 1259.

28.   Conti, M.; Donati, G.; Cianciolo, G.; Stefoni, S.; Samori, B.   *J. Biomed. Mater. Res.*, **2002**, 61, 370.

29.   Cheng, S.; Chitttur, K.; Sukenik, C.; Culp, L.; Lewandowska, K.   *J. Colloid Interface Sci.*, **1994**, 162, 135.

30.   Culp, L. A.; Sukenik, C. N. *J. Biomater. Sci. Polym. Ed.,* **1998**, 9, 1161.

31.   Binnig, G.; Quate, C. F.; Gerber, C. *Phys. Rev. Lett.*, **1986**, 56, 930.

32.   Florin, E.; Moy, V. T.; Gaub, H. E. *Science.* **1994**, 264, 415.

33.   Bemis, J.; Akhremitchev, B.; Walker, G. *Langmuir.* **1999**, 15, 2799.

34.   Smith, B. L.; Schaeffer, T. E.; Viani, M.; Thompson, J. B.; Frederick, N. A.; Kindt, J.; Belcher, A.; Stucky, G. D.; Morse, D. E.; Hansma, P. K. *Nature* **1999**, 399, 761.

35.   Zhang, W. K.; Zou, S.; Wang, C.; Zhang, X. J. *J. Phys. Chem. B* **2000**, 104, 10258.

36.   Al-Maawali, S.; Bemis, J. E.; Akhremitchev, B. B.; Leecharoen, R.; Janesko, B. G.; Walker, G. C. *J. Phys. Chem. B*. **2001**, 105, 3965.

37.   Ortiz, C.; Hadziioannou, G. *Macromolecules.* **1999**, 32, 780; Schonherr, H.; Beulen, M. W. J.; van Veggel, F. C. J. M.; Bugler, J.; Huskens, J.; Reinhoudt, D. N.; Vancso, G. J. *J. Am. Chem. Soc*. **2000**, 122, 4963.

38. Kellermayer, M. S. Z.; Smith, S. B.; Bustamante, C.; Granzier, H. L. *Biophys. J.* **2001**, 80, 852.

39. Tskhovrebova, L.; Trinick, J.; Sleep, J. A.; Simmons, R. M. *Nature*. **1997**, 387, 308.

40. Rief, M.; Gautel, M.; Oesterhelt, F.; Fernandez, J. M.; Gaub, H. E. *Science*. **1997**, 276, 1109; Gale, M., Pollanen, M. S., Markiewicz, P.; Goh, M. C. *Biophys. J.*, **1995**, 68, 2124.

41. Oberhauser, A. F.; Marszalek, P. E.; Erickson, H. P.; Fernandez, J. M. *Nature*. **1998**, 393, 181.

42. Law, R.; Carl, P.; Harper, S.; Dalhaimer, S.; Speicher, D. W.; Discher, D. E. *Biophys. J.* **2003**, 84, 533.

43. Strunz, T.; Oroszlan, K.; Schafer, R.; Guntherodt, H. *Proc. Natl. Acad. Sci.* **1999**, 96, 11277.

44. Liphardt, J.; Onoa, B.; Smith, S.B.; Tinoco Jr., I.; Bustamante, C. *Science*. **2001**, 292, 733.

45. Bell, G.I. *Science*. **1978**, 200, 618.

46. Evans, E. *Annu. Rev. Biophys. Biomol. Struct*. **2001**, 30, 105.

47. Evans, E. *Faraday Discuss*. **1998**, 111, 1.

48. Evans, E.; Ludwig, F. *J. Phys.: Condens. Matter* **2000**, 12, A315.

49. Evans, E.; Ritchie, K. *Biophys. J.* **1999**, 76, 2439.

50. Merkel, R.; Nassoy, P.; Leung, A.; Ritchie, K.; Evans, E. *Nature* **1999**, 397, 50.

51. Evans, E.; Ritchie, K. *Biophys. J.* **1997**, 72, 1541.

52. Strunz, T.; Oroszlan, K.; Schumakovitch, I.; Guntherodt, H. J.; Hegner, M. *Biophys. J.* **2000**, 79, 1206.

53. Dettmann, W.; Grandbois, M.; Andre, S.; Benoit, M.; Wehle, A. K.; Kaltner, H.; Gabius, H.; Gaub, H. E. *Arch. Biochem. Biophys*. **2000**, 383, 157.

54. Hummer, G.; Szabo, A. *Biophys. J.*, **2003**, 85, 5.

55. Groth, T.; Altankov, G.; *J. Biomater. Sci. Polym. Ed.*, **1995**, 7, 297.

56. Altankov, G.; Grinnell, F.; Groth, T. *J. Biomed. Mater. Res.*, **1996**, 30, 385.

57. Grinnell, F.; Feld, M. K. *J. Biomed. Mater. Res.*, **1981**, 15, 363.

58. Hegner, M.; Wagner, P.; Semenza, G. *Surface Science*, **1993**, 291, 39.

59. Butt, H-J; Jaschke, M; *Nanotechnology*, **1995**, 6, 1.

60. Rief, M.; Gautel, M.; Oesterhelt, F.; Fernandez, J.M.; Gaub, H.E. *Science*. **1997**, 276, 1109.

61. Carrion-Vasquez, M.; Oberhauser, A.F.; Fowler, S.B.; Marszalek, P.E.; Broedel, S.E.B.; Clarke, J.; Fernandez, J.M. *Proc. Natl. Acad. Sci*. **1999**, 96, 3694.

62. Zhou, Y.; Nagaoka, T.; Zhu, G. *Biophys. J*. **1999**, 79, 55.

63. Sukhishvilli, S. A.; Chen, Y.; Mueller, J. D.; Gratton, E.; Schweizer, K. S.; Granick, S. *Nature* **2000,** 404, 146.

64. Jacob, M.; Schmid, F.X. *Biochemistry* **1999**, 38, 13773.

65. Swegat, W.; Schlitter, J.; Kruger, P.; Wollmer, A. *Biophys. J*. **2003**, 84, 1493.

66. Portman, J.J.; Takada, S.; Wolynes, P.G. *J. Chem. Phys*. **2001**, 114, 5082.

67. Plaxco, K.W.; Baker, D. *Proc. Natl. Acad. Sci*. **1998**, 95, 13591.

68. Alm, E.; Morozov, A.V.; Kortemme, T.; Baker, D. *J. Mol. Biol*. **2002**, 322, 463.

69. Ghatak, A.; Vorvolakos, K.; She, H.; Malotky, D.; Chaudhury, M.K. *J. Phys. Chem. B* **2000**, 104, 4018.

70. Jeon, S.I.; Andrade, J.D. *J. Colloid Interface Sci*. **1991**, 142, 159.

71. Jeon, S.I.; Lee, J.H.; Andrade, J.D.; De Gennes, P.G. *J. Colloid Interface Sci*. **1991**, 142, 149.

72. Bjorling, M. *Macromolecules*. **1992**, 25, 3956.

73. Isreals, R.; Leermakers, F.A.M.; Fleer, G.J. *Macromolecules*. **1995**, 28, 1626.

74. Desai, N. P.; Hubbell, J. A. *Biomaterials*, **1991**, 12, 144.

75. Gombotz, W. R.; Wang, G.; Horbett, T. A.; Hoffman, A. S. *J. Biomed. Mater. Res.*, **1991**, 25, 1547.

76. Wertz, C. F.; Santore, M. M. *Langmuir*, **2001**, 17, 3006.

PREFACE

As we saw in the last chapters, AFM allows us to determine the thermodynamic parameters involved in mechanically denaturing a protein as well as its dissociation from a surface. Because of the distinct values obtained, we then explored whether AFM could be used to identify the polymer block that is bound to our AFM probe in a diblock system. The next chapter describes our results from elongating a diblock system of polystyrene-poly-2-vinylpyridine from a glass substrate. We also elongated pure polystyrene and poly-2-vinylpyridine for our controls. Our results show that the AFM can be used to reveal the nature of the surface-macromolecule contact.

4. QUANTIFYING ADHESION BOND PARAMETERS TO DISTINGUISH INTERACTIONS OF HYDROPHILIC AND HYDROPHOBIC BLOCKS OF POLYSTYRENE-POLY-2-VINYLPYRIDINE WITH A SILICON NITRIDE SURFACE[3]

An analysis of the loading rate dependence of the forces required to rupture an AFM tip from a block copolymer surface has provided insight into the structure of the surface-macromolecule contact, differentiation of the block contacting the tip, a measure of the polymer-surface binding energy, and the rigidity of the contact. Polystyrene-poly-2-vinylpyridine block copolymers were studied adsorbing to silicon nitride. Polystyrene makes stiff van der Waals contact with the silicon nitride surface in aqueous solution while the bond of poly-2-vinyl pyridine to the surface is more flexible and may involve a bridging water.

An analysis of the loading rate dependence of the forces required to rupture an AFM tip from a block copolymer surface is reported that provides insight into the structure of the surface-macromolecule contact, differentiation of the block contacting the tip, a measure of the polymer-surface binding energy, and the rigidity of the contact. In a poor solvent, a macromolecule may be driven entirely into contact with a surface if the interaction with the surface is favorable while in a good solvent, the chain dissolves or at least exhibits large fractions extended into solution.[1] Macromolecular adhesion to surfaces is at the foundation of numerous polymer-based technologies and natural biomaterial interfaces,[2] yet adhesion bond measurements to compare with predictive models have often proven elusive.

Molecular force spectroscopy,[3-12] which probes conformational transitions as a function of structural loading rate, potentially provides the ability to examine the structure of macromolecule-surface bonds directly. The unloading rate dependence of the adhesion between the AFM tip and the molecule should provide information that is significantly beyond adhesion strength. The force required to rupture a polymer chain from an interacting molecular force probe is illustrated in the inset of Figure 18. In a simple model initially proposed by Bell and Evans,[13] each linear region seen in a plot of the transition force *versus* the logarithm of the loading rate corresponds to a barrier traversed by the system in the direction of applied force. From the slopes and intercepts of each linear region, information about barrier heights, barrier positions for bond breaking as well as rates of reaction can be calculated. Recently, a more accurate method was proposed by Hummer and Szabo.[14] Here, we report experimental rupture data, analyzed by the Hummer model, to characterize the diblock copolymer interactions with a silicon nitride AFM tip. This paper provides a description of the surface unbinding of individual polymer blocks under conditions where a specific solvent-polymer-surface structure is expected.
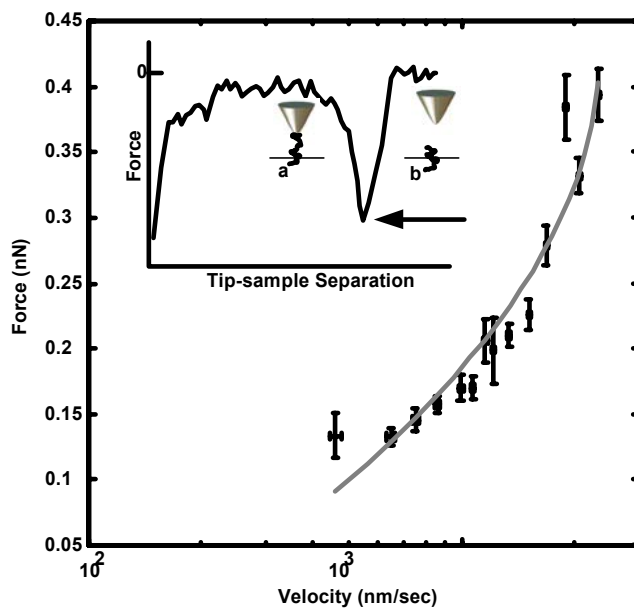
Figure 18 Inset: Force-extension data for a polymer chain (a) being stretched away from the surface by the AFM tip. After the rupture of the adhesive bond (arrow), the interaction force falls to zero (b). Outset: A fit of the Hummer model (gray line) to the polystyrene-surface bond rupture force as a function of the velocity of the separation of the two surfaces.

Films of the named polymers were spun cast from THF solution onto glass substrates and examined under 10mM sodium acetate solution, as described previously.[15] The surface topography of the block copolymers is irregular with occasional features about 100 nm tall. Smaller (~50 nm wide, 5 nm high), more ordered structures which appear micellar in nature,[15-17] are also visible. These micellar structures are not visible in the homopolymer studies. In the ample areas (~1μm^2) that are devoid of height features greater than 15 nm, force-distance plots were then collected. The magnitude of the rupture force as a function of the loading rate was then obtained.

These data were analyzed using Hummer's method to characterize the adhesion reaction surface (See Figure 19). In the Hummer model, the bond is loaded by a flexible chain,[18] and the bond is characterized by a harmonic potential with a cut-off at a critical barrier position and

height where the loaded bond ruptures. The molecular spring constant $k_m{}^*$ illustrates the stiffness of the adhesive bond, and free motion on the reaction surface is characterized by a diffusion coefficient, D.[19]
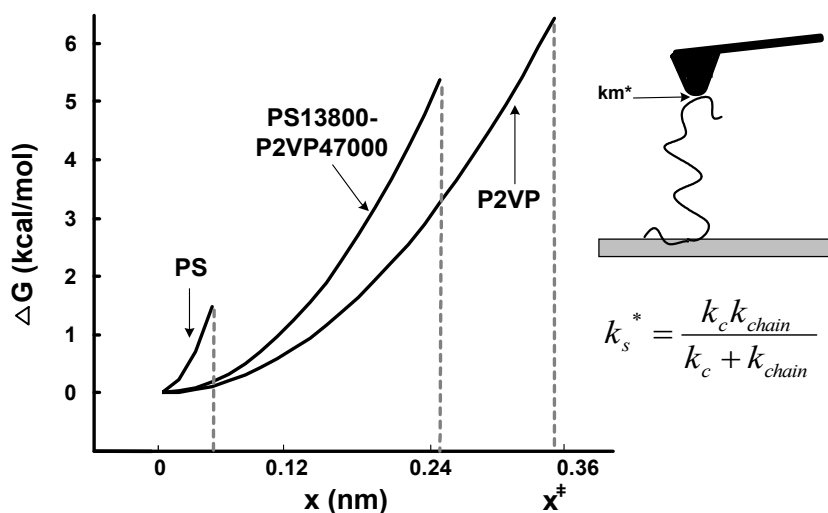
Figure 19 Left. Free energy surfaces and transition positions in the bond extension coordinate shown for polystyrene (PS), Poly-2-vinylpyridine (P2VP), and a block copolymer separating from a silicon nitride tip in aqueous buffer. ΔG offsets between curves are unknown. Upper right. Scheme of polymer-AFM tip bond being loaded, broken, and analyzed. Stiffness of polymer-tip surface bond is $k_m{}^*$. Lower right. Bond is loaded by a spring of stiffness $k_s{}^*$ comprised of cantilever and polymer chain springs.

Table 13 Thermodynamic and Kinetic Parameters Obtained for PS, P2VP, and Their Diblock Copolymers Detaching From a Silicon Nitride Surface

Molecule	k_m^* (N/m)	$x^{\ddagger}$ (nm)	$\Delta G^{\ddagger}$ (kcal/mol)	$k_{off}(0)$ (sec^{-1})	k_{chain} (N/m)	D (nm^2/s)
PS29100	6.4	0.06	1.5	83	0.62	0.80
P2VP50000	0.75	0.35	6.5	0.4	0.03	69
PS7800-P2VP10000	0.82	0.34	6.9	0.12	0.14	41
PS13800-P2VP47000	1.2	0.25	5.4	1.6	0.08	31
PS60100-P2VP46900	0.91	0.25	4.0	7.2	0.04	19

An analysis for rupturing different PS and P2VP adhesion bonds with a silicon nitride surface is summarized in Table 13. It can be seen that the stiffness of the adhesion bond for pure polystyrene is nearly ten times that of pure P2VP and the diblock copolymers while the barrier to breaking the adhesion bond is nearly six times smaller. From this data, we infer that the P2VP block of the diblock copolymers is preferentially exposed to the aqueous solution. This is reasonable given the polar nature of P2VP and the non-polar nature of PS. In addition, we observe that the distance to the barrier is significantly greater for rupturing the P2VP–surface bond compared with the PS-surface bond. This, we speculate, is due to two different characteristic polymer-Si_3N_4 surface bonds. In the case of PS, it appears that a tight bond, probably caused by a direct van der Waals attraction with a neutral region of the AFM tip's surface, is present. The surface charge density on a silicon nitride tip at pH 7 is -0.03 e/nm^2, determined by measuring the surface feature's apparent height at different electrolyte concentrations, which provides free space for polymer binding to neutral regions.[20] On the other hand, P2VP would be expected to bind preferentially to surface silanols. The far greater distance

to the barrier and the softness of the effective spring suggests the P2VP-surface bond occurs through another surface intermediate, perhaps a water molecule bound to a surface silanol.

This description of an indirect interaction between a pyridine ring and silica surface is consistent with observations from other researchers, though our work may provide the first direct evidence. Yoon and coworkers[21] found by AFM that the hydration force between a silicon nitride tip and silica surface remains unchanged in 2% pyridine in water. Matzner *et al.*[22] determined the standard free energy of adsorption (ΔG^o_{ads}) for pyridine binding to silica is -14 kJ/mol. Since this value is smaller than the heat of adsorption of water vapor on silica (52 kJ/mol),[23] it was suggested that pyridine may adsorb on silica in such a way that the water molecules are not displaced from the first (few) adsorption layer(s). Upon adsorption to a silica surface, only weak perturbation of pyridine's Raman spectrum was observed.[22] Rivera and Harris[24] found that pyridine bound via waters bound to surface silanols of silica sol-gels with a free energy of adsorption of 13.0 +/- 2.5 kJ/mol.

The fitted diffusion coefficients for PS on silicon nitride are about 25-75 times smaller than that of P2VP. These values are comparable to those previously obtained by other means $(0.02 -0.26 \text{ nm}^2/s)$.[25]

In this work, it is not determined how many individual "contact points" there are between a chain and the surface at rupture, though the heights of the barriers to unbinding are consistent with a single contact. If the number of contacts is different between the polymer blocks and the surface, then the rupture process might not be viewed as breaking a single contact which could affect the molecular interpretation of the barrier positions obtained by the Hummer model, though a full discussion of this effect is beyond the scope of this paper.

BIBLIOGRAPHY

1.   Lin, Z.; Kim, D. H.; Boosahda, L.; Stone, D.; LaRose, L. ; Russell, T. P. *Adv. Mat.,* **2002***, 14, 1373; Xu, T.; Russell, T. P.; Hawker, C. J. *Macromol.* **2003**, 36, 6178.

2.   Israelachvili, J. *Intermolecular and Surface Forces*, 2nd ed.; Academic press: San Diego, 1992.

3.   Meadows, P.Y.; Bemis, J.E.; Walker, G.C. *Langmuir* **2003**, 19, 9566.

4.   Ikai, A.; Afrin, R. *Cell Biochem. Biophys*. **2003**, 39, 257

5.   Oberhauser, A.F.; Badilla-Fernandez, C.; Carrion-Vazquez, M.; Fernandez, J.M. *J. Mol. Biol*. **2002**, 319, 433.

6.   Dettmann, W.; Grandbois, M.; Andre, S.; Benoit, M.; Wehle, A.K.; Kaltner, H.; Gabius, H.; Gaub, H.E. *Arch. Biochem. Biophys*. **2000**, 383, 157.

7.   Rief, M.; Grubmueller, H.; *Chem. Phys. Chem.* **2002**, 3, 255.

8.   Cui, S.; Liu, C.; Wang, Z.; Zhang, X.; Strandman, S.; Tenhu, H. *Macromol.* **2004**, 37, 946.

9.   Law, R.; Carl, P.; Harper, S.; Dalhaimer, P.; Speicher, D. W.; Discher, D. E. *Biophysical J.* **2003,** 84, 533.

10.   Auletta, T.; de Jong, M. R.; Mulder, A.; van Veggel, F. C. J. M. Jurriaan Huskens; Reinhoudt, D. N.; Zou, S.; Zapotoczny, S.; Schönherr, H.; Vancso, G. J.; Kuipers, L. *J. Am. Chem. Soc.* **2004**, 126, 1577.

11.   Kokkoli, E.; Ochsenhirt, S. E.; Tirrell, M. *Langmuir*, 2004, 20, 2397.

12.   Ghatak, A.; Vorvolakos, K.; She, H.; Malotky, D. Chaudhury, M. K *J. Phys Chem B* **2000**, 104, 4018.

13.   Bell, G. I. *Science*. **1978**, 200, 618.; Evans, E. *Annu. Rev. Biophys. Biomol. Struct*. **2001**, 30, 105; Evans, E. *Faraday Discuss*. **1998**, 111, 1; Evans, E.; Ludwig, F. *J. Phys.: Condens. Matter* **2000**, 12, A315.; Evans, E.; Ritchie, K. *Biophys. J*. **1999**, 76, 2439; Merkel, R.; Nassoy, P.; Leung, A.; Ritchie, K.; Evans, E. *Nature* **1999**, 397, 50; Evans, E.; Ritchie, K. *Biophys. J*. **1997**, 72, 1541.

14. Hummer, G.; Szabo, A. *Biophys. J* . **2003**, 85, 5.

15. Bemis, J.E.; Akhremitchev, B.B., Walker, G.C. *Langmuir* **1999**, 15, 2799.

16. Stamouli, A.; Pelletier, E.; Koutsos, V.; Vegte, E. V. D.; Hadziioannou, G. *Langmuir*, **1996**, *12*, 3221-3224.

17. Talingting, M.; Munk, P.; Webber, S.; Tuzar Z. *Macromol.* **1999**, 32, 1593.

18. Ortiz, C.; Hadziioannou, G. *Macromolecules* **1999**, 32, 780.

19. In the model, the free energy surface is harmonic with a cut-off:

$$ß\, V_o(x) = 1/2\, k_m\, x^2 \quad \text{for } (x < x^{\ddagger}) \text{ and } ß\, V_o(x) = -\infty \quad \text{for } (x > x^{\ddagger})$$

Here k_m is the molecular spring constant and x is a good reaction coordinate if the dynamics of the other degrees of freedom are sufficiently fast. $ß = k_B T$. $ß k_m = k_m{}^*$, and $ß k_s = k_s{}^*$.   The average rupture force *versus* velocity data are then fit by $\beta F = k_m x^{\ddagger} - [2k \ln\{k_{off}(0) \exp(\gamma + k_m(x^{\ddagger})^2/2) / k_s\, v\, x^{\ddagger}\, (k_m/k)^{3/2}\}]^{1/2}$. Here $k = k_m + k_s$, where k_s is the pulling spring constant and reflects the properties of the cantilever and polymer chain linker. The loading rate was obtained directly from our force plots using four data points prior to the cantilever's point of maximum extension. The velocity is then calculated using the loading rate and spring constant of the system. Therefore, a factor of $\{1 + (k_c k_m + k_c k_{chain})/(k_m k_{chain})\}$ was multiplied to v in the above equation to account for the tip's velocity.

20. Muller, DJ; Engel, A. *Biophys. J.* **1997**, 73, 1633.

21. Yoon, R.-H.; Vivek, S., *J. Colloid Interface Sci.***1998**, 204 , 179.

22. Matzner, R.A.; Bales, R.C.; Pemberton, J. E. *Appl. Spectr.* **1994**, 48**,** 1043.

23. Jones, D. C.; Mill, G. S. *J. Chem. Soc.* **1957**, 213.

24. Rivera, D. Harris, J. M. *Langmuir*, **2001**, 17, 5527.

25. Wertz, C. F.; Santore, M. M. *Langmuir*, **2001**, 17, 3006.

5.   CONCLUDING REMARKS

In the previous chapters, we have used an AFM to study the mechanical properties of fibronectin and copolymer systems. In Chapter 2, the AFM was used primarily as a single molecule force probe to obtain information about FN's stability as a function of protein concentration. To our knowledge, we are the first ones to show the mechanical behavior of an isolated protein adsorbed to a substrate. Most literature uses force volumes which randomly sample the surface and does not allow the force plots to be associated with a specific adsorbed protein nor can it be conclusively shown that the protein was isolated on the substrate. From our results, we have shown that when elongating single molecules of FN on a mica surface, the protein is already predenatured on the surface prior to its extension. Only upon increased surface coverage does the protein remain folded before it is extended. The ruptures observed in our single molecule work, although not domain unfolding events, appear to correspond to a specific protein-surface interaction.

In Chapter 3, we continued our studies of FN but this time on a variety of different substrates. For this work, we created two surface conditions for FN: an aggregated and semiaggregated environment. Modeling of the data using two different theories resulted in similar trends for the fitted thermodynamic parameters. Insight into the protein's binding state could then be obtained. Aggregated proteins adsorbed on hydrophobic surfaces adopted more rigid conformations due to increased surface denaturation and tighter binding while looser conformations were observed on the more hydrophilic surfaces. Interestingly, studies of FN in a

semiaggregate state showed heterogeneity in the models' thermodynamic parameters suggesting that in the early stages of nonspecific adsorption, multiple protein conformations exist, each having bound irreversibly to the substrate. An estimation of the spring constant of these proteins showed more rigid conformations than in the corresponding aggregate work due to the greater number of substrate contacts available to the protein. Finally, we seeded these substrates with human umbilical vascular endothelial cells. As predicted from the models used in this work, surfaces with aggregated FN promoted cellular deposition while surfaces with FN in a semiaggregate form hindered cell deposition and growth. Several studies indicate that the ability of cells to "recognize" a surface does depend on the protein's surface coverage. Very hydrophilic surfaces may not be as favorable for cell adsorption because few proteins have been found on these substrates. On the other hand, very hydrophobic surfaces which have numerous proteins are not favorable because the proteins are more tightly bound. Surfaces between these extremes are better suited for cell seeding. Our results show PEG, a hydrophilic surface, to inhibit proteins from adsorbing while the more hydrophobic surfaces have more rigid protein conformations. Further testing is needed to shed light on an AFM's ability to project a surface's suitability for seeding experiments, but initial results do look promising.

In Chapter 4, we began examining systems of polystyrene-poly-2-vinylpyridine. An analysis of the loading rate dependence of the forces required to rupture an AFM tip from these block copolymer surfaces gave insight into the surface-macromolecular contact. The specific block bound to the AFM probe, the rigidity of the contact, and the molecule's diffusion coefficient could be obtained through this analysis.

In this work, we used AFM primarily as a single molecule force probe where we obtained information about the thermodynamics of adsorbed protein and polymer surfaces. Future studies

can continue to explore AFM's ability to project cell seeding and later biocompatibility measurements. Additionally, studies where information is needed on a multi-component system can use the method described in Chapter 4 to identify the molecule exposed on the surface. Thus, future studies could use AFM as a "fingerprinting" tool.